Supplementary Information

Twin Interfacial Charge Channels Enable Efficient Photorefining of Raw Biomass

Fuyan Kang[a, b, d], Chao Xu[c], Chengfang Wang[a], Zhanhua Huang[a, *], Hongwei Ma[b, *], Chaoji Chen[c, *], Jinguang Hu[d,*]

[a] Key Laboratory of Bio-based Material Science and Technology, Ministry of Education, Material Science and Engineering College, Northeast Forestry University, Harbin 150040, Heilongjiang, China

[b] Department of Chemistry and Chemical Engineering, College of Chemistry, Chemical Engineering and Resource Utilization, Northeast Forestry University, Harbin 150040, P. R. China

[c] Hubei Key Laboratory of Biomass Resource Chemistry and Environmental Biotechnology, School of Resource and Environmental Science, Wuhan University, Wuhan 430079, P. R. China

[d] Department of Chemical and Petroleum Engineering, University of Calgary, 2500 University Drive, NW, 2500 University Drive, NW, Calgary, Alberta, T2N 1N4, Canada

[*]Email: huangzh1975@163.com; mahw@nefu.edu.cn; chenchaojili@whu.edu.cn; jinguang.hu@ucalgary.ca.

Experimental Section

Synthesis of ZnS(en)

ZnS(en) was synthesized by a simple solvothermal method. Typically, 2 mmol of zinc acetate and 6 mmol of thiourea are dispersed in 30 mL of ethylenediamine solution. The mixed solution was stirred at room temperature for 30 min. Subsequently, the mixed solution is transferred to teflon lined and reacted for 12 h at 160 ℃. Samples are collected, washed and dried. The prepared samples were noted as ZnS(en). In the similar experimental steps, the samples prepared with the solvent as water were noted as ZnS.

Preparation of CdS

2 mmol of cadmium acetate and 6 mmol of thiourea were added to 30 mL of ethylenediamine solution. The mixed solution was stirred at room temperature for 60 min. Subsequently, the solution was transferred to the reactor and reacted for 8 h at 100 ℃. The catalyst is collected and washed, dried. The catalyst prepared is denoted as CdS.

Supplemental Figures and Tables

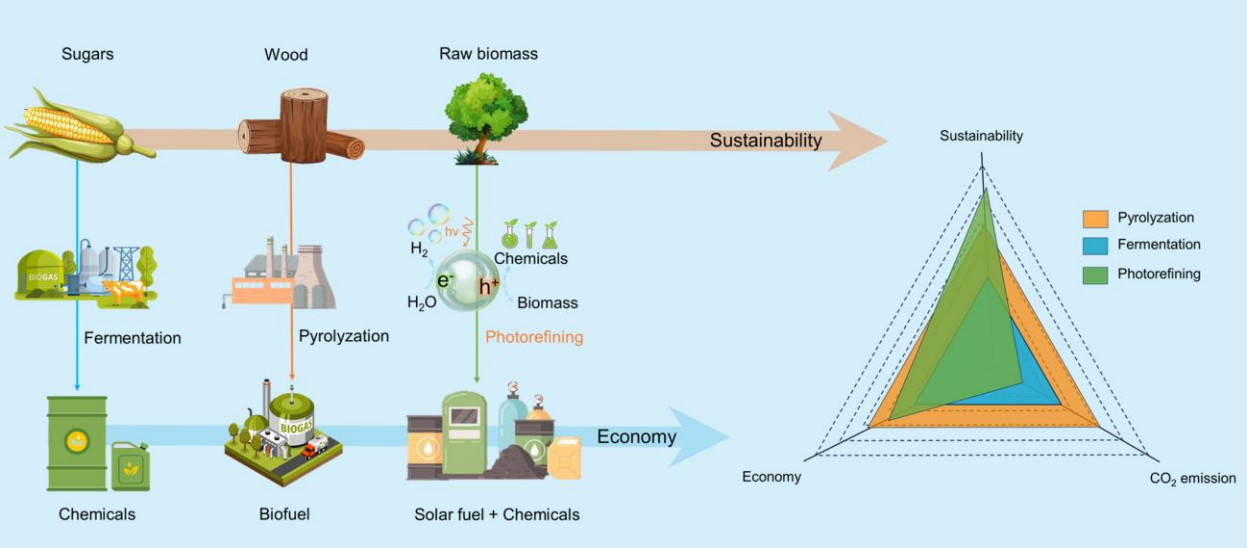

Fig. S1 Advantages of photorefining technology compared to traditional biomass conversion techniques. The processes and primary products of biomass valorization by fermentation, pyrolysis, and photorefineries. Biomass photorefining can efficiently produce solar fuels and platform chemicals at the same time, making the technology more valuable.

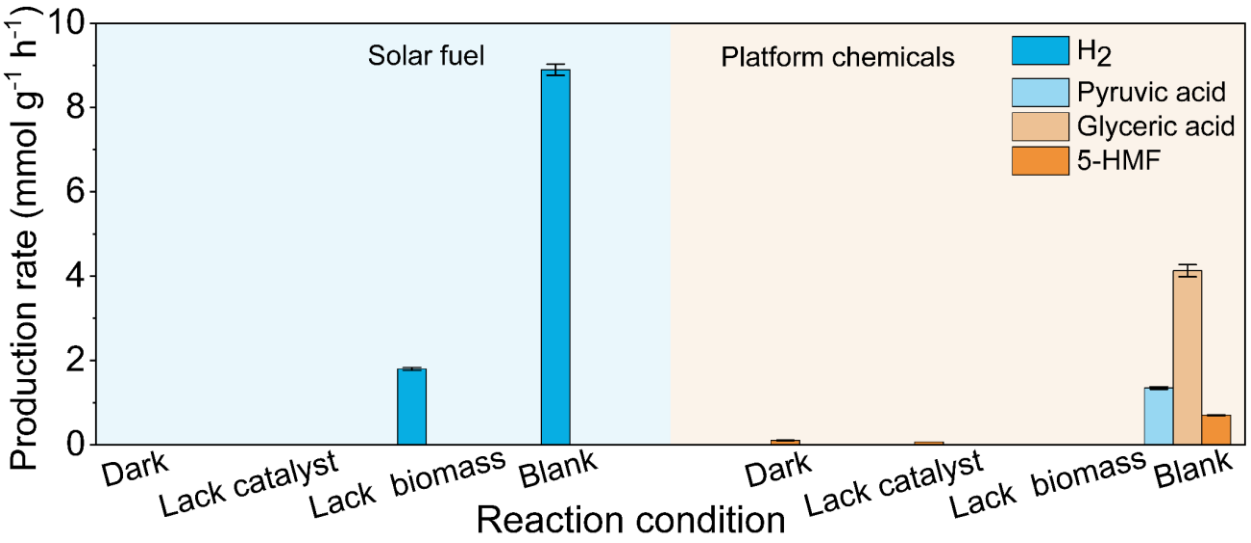

Fig. S2. Hydrogen and platform compound generation rates of condition comparison experiment experiments. The photorefining rate of the cyclic experiment. Photorefining reaction conditions: 100 mg bagasse, 25 mg catalyst, DMSO:water = 25 mL: 25 mL, 5 g NaOH and 300 W xenon lamp as the light source.

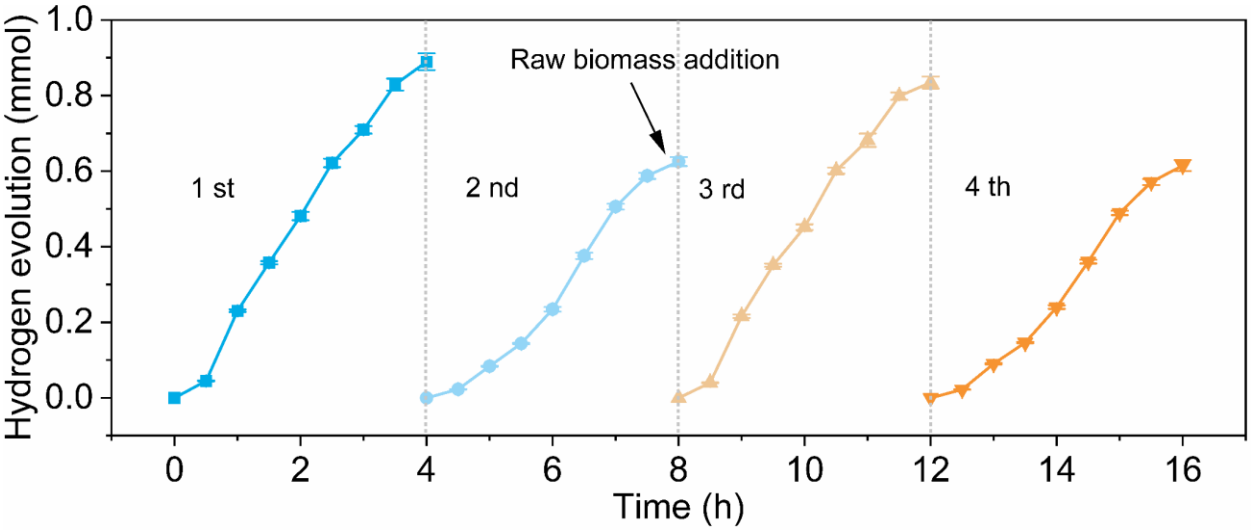

Fig. S3. Stability investigation of the hydrogen cycle in raw biomass photorefining with ZnS(en)/CdS-3. Hydrogen evolution in cyclic experiments. Photorefining reaction conditions: 100 mg bagasse, 25 mg catalyst, DMSO:water = 25 mL: 25 mL, 5 g NaOH, reaction time: 4 h and 300 W xenon lamp as the light source.

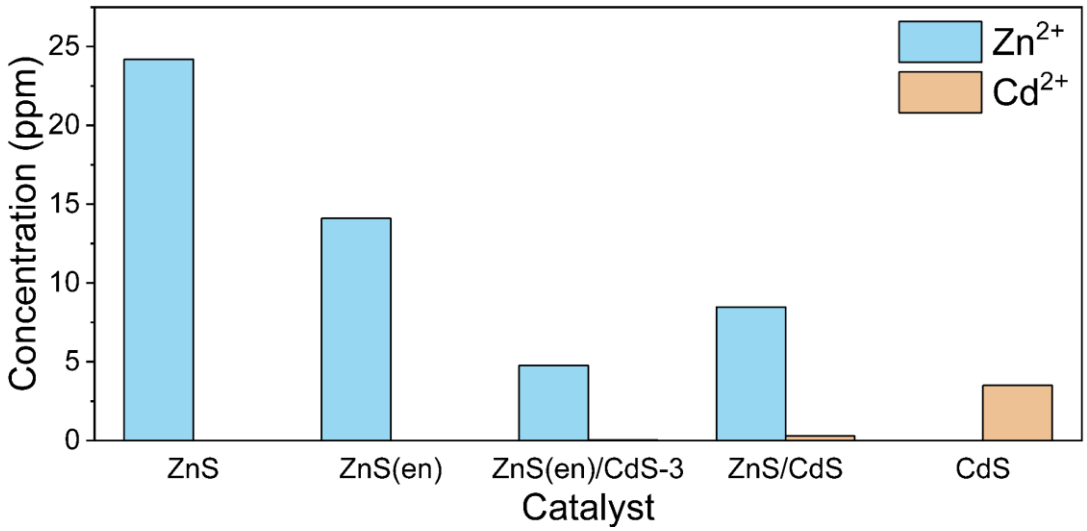

Fig. S4. Stability investigation of the hydrogen cycle in raw biomass photorefining with ZnS(en)/CdS-3. Hydrogen evolution in cyclic experiments.

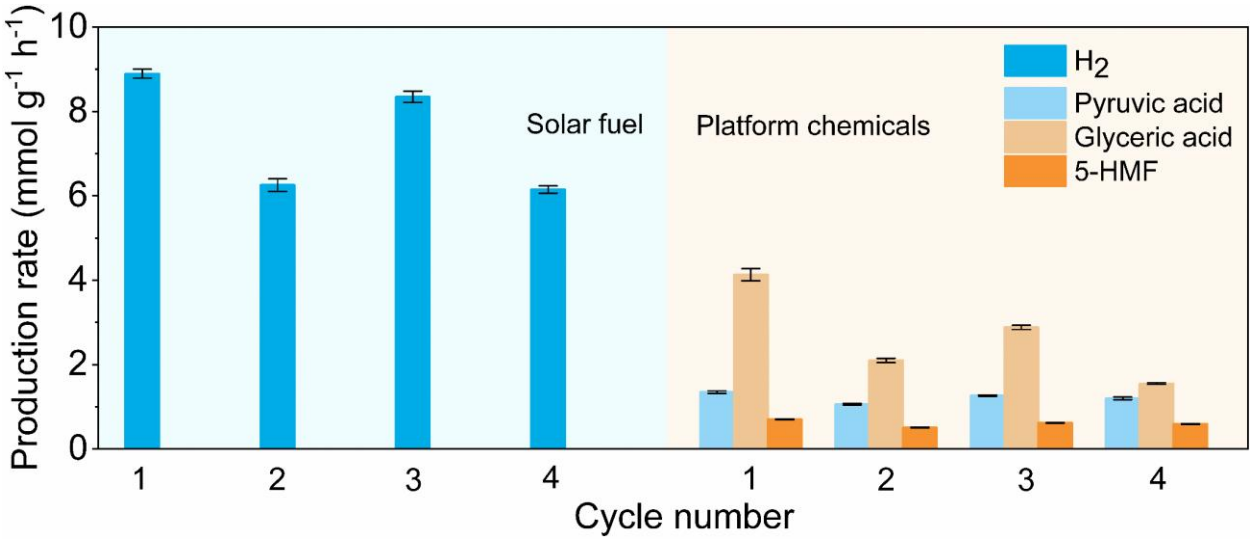

Fig. S5. Hydrogen and platform compound generation rates of composites in cyclic stability experiments. The photorefining rate of the cyclic experiment. Photorefining reaction conditions: 100 mg bagasse, 25 mg catalyst, DMSO:water = 25 mL: 25 mL, 5 g NaOH, reaction time: 4 h and 300 W xenon lamp as the light source.

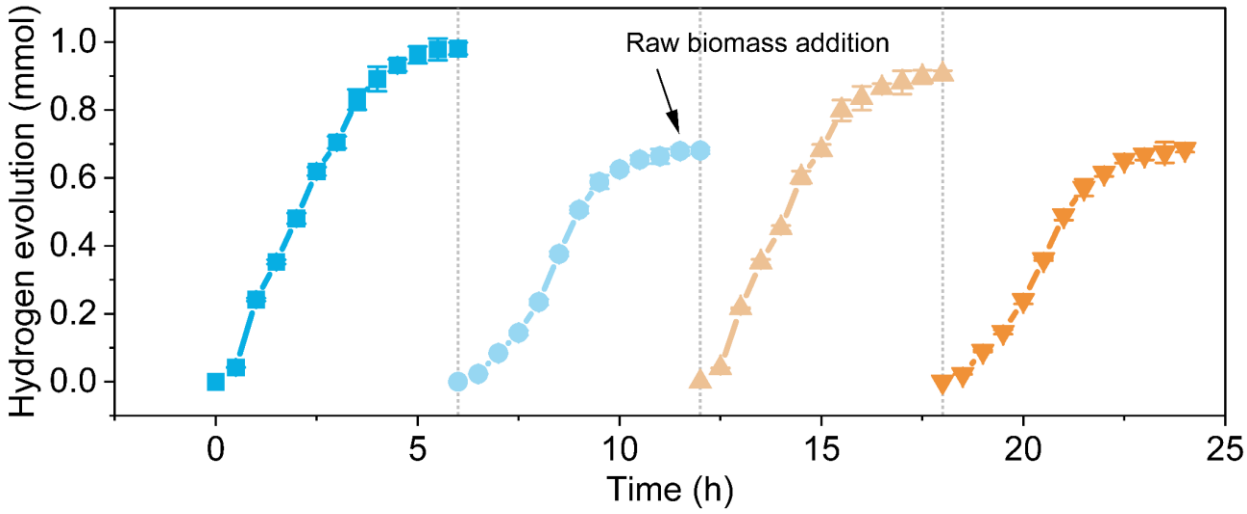

Fig. S6. Photocatalytic hydrogen evolution with extended cycle time to 6 hours. Hydrogen evolution in cyclic experiments for Zn(en)/CdS-3. Photorefining reaction conditions: 100 mg bagasse, 25 mg catalyst, DMSO:water = 25 mL: 25 mL, 5 g NaOH, reaction time: 4 h and 300 W xenon lamp as the light source.

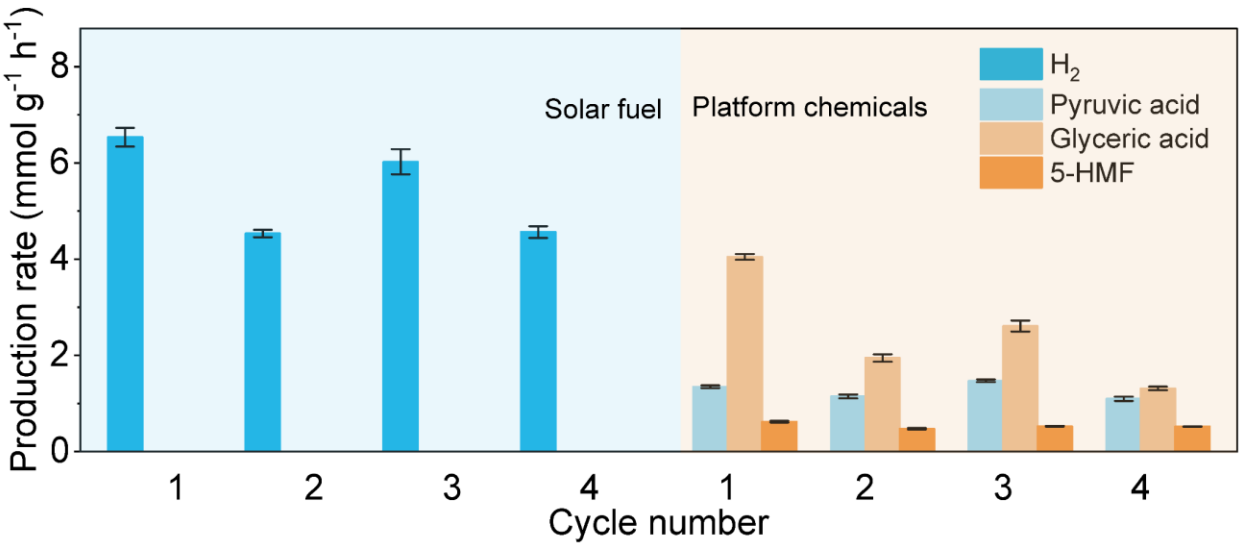

Fig. S7. Hydrogen and platform compound generation rates with extended cycle time to 6 hours for Zn(en)/CdS-3. The photorefining rate of the cyclic experiment. Photorefining reaction conditions: 100 mg bagasse, 25 mg catalyst, DMSO:water = 25 mL: 25 mL, 5 g NaOH, reaction time: 6 h and 300 W xenon lamp as the light source.

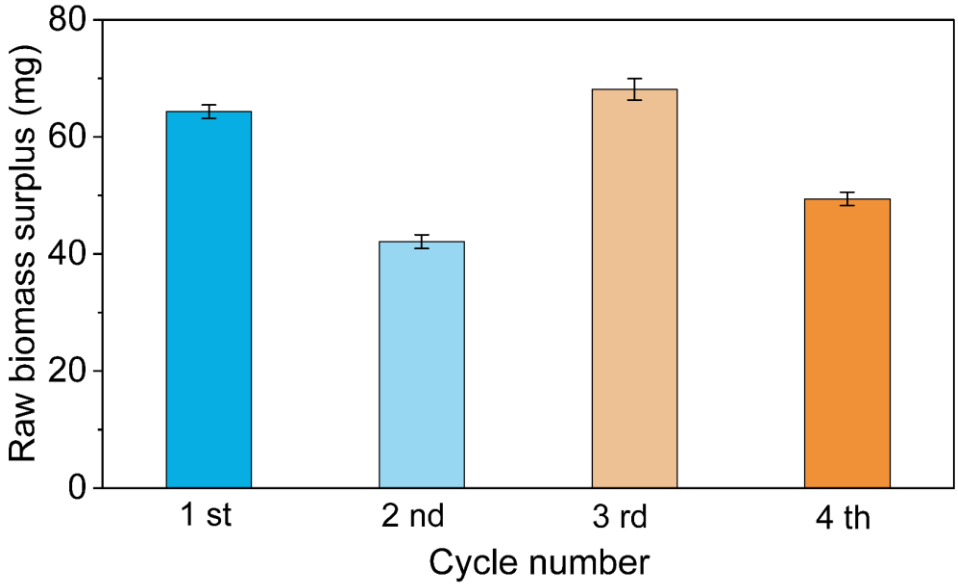

Fig. S8. Raw biomass surplus in recycling experiments. After the second cycle of the experiment, the reaction system was added with 50 mg of raw biomass. Photorefining reaction conditions: 100 mg bagasse, 25 mg catalyst, DMSO:water = 25 mL: 25 mL, 5 g NaOH, reaction time: 4 h and 300 W xenon lamp as the light source.

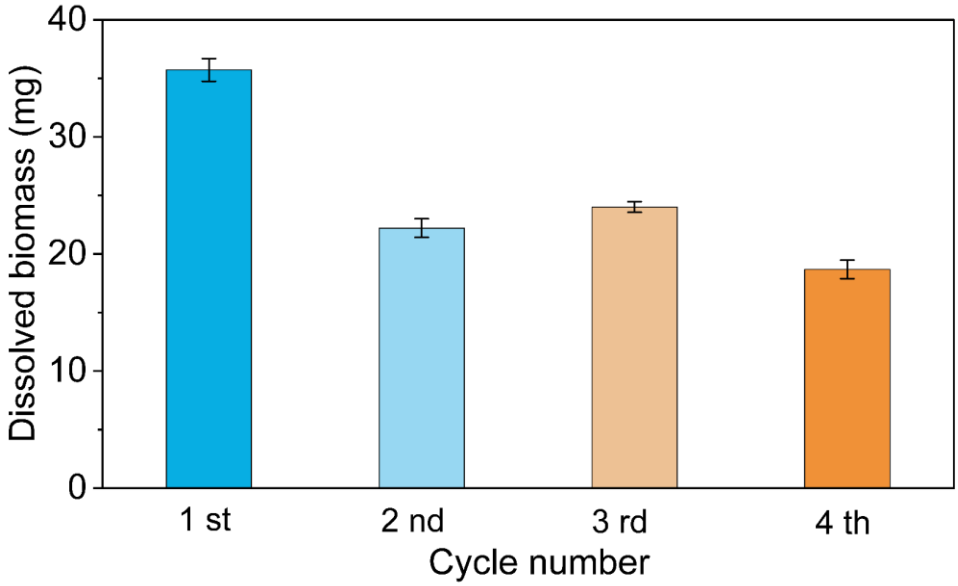

Fig. S9. Dissolved biomass in recycling experiments. After the second cycle of the experiment, the reaction system was added with 50 mg of raw biomass. Photorefining reaction conditions: 100 mg bagasse, 25 mg catalyst, DMSO:water = 25 mL: 25 mL, 5 g NaOH, reaction time: 4 h and 300 W xenon lamp as the light source.

Table S1 The main component of lignocellulose (%).

Samplesa	Cellulose	Hemicellulose	Lignin		Ash
			Acid soluble lignin	Acid insoluble lignin	
Bagasse before reaction[a]	36.57 %	24.87 %	4.25 %	18.74 %	7.20 %
Bagasse after reaction[b]	52.77 %	10.33 %	4.68 %	13.32 %	10.23 %

a Determination of lignocellulosic component content by NREL method.

b This content is expressed as a percentage relative to the total mass.

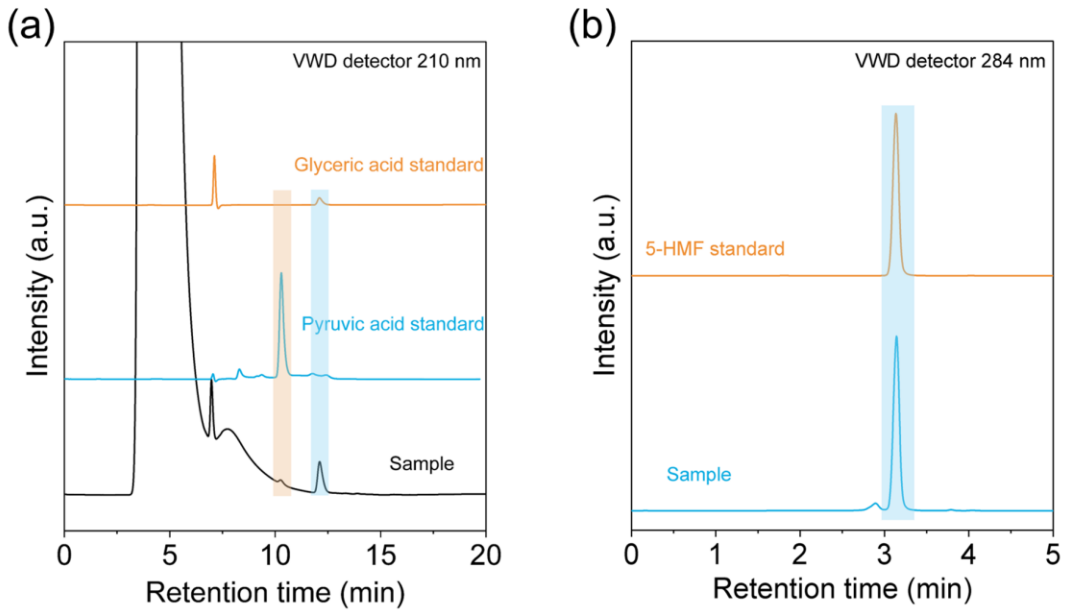

Fig. S10. Comparison of the spectra of the samples with those of the standard liquid chromatography samples. Sample reaction conditions were: 25 mg catalyst, 100 mg bagasse, 2.5 M NaOH in a mixed solution of DMSO and water (V:V=1:1), light reaction for 4 h. Detection at different wavelengths with Variable Wavelength Detector (VWD).

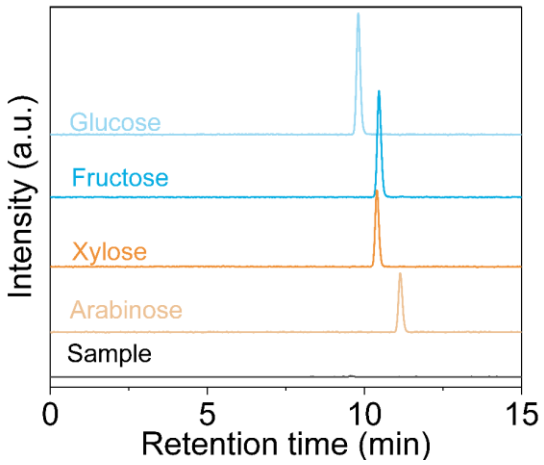

Fig. S11. Comparison of the spectra of the samples with those of the standard liquid chromatography samples. Sample reaction conditions were: 25 mg catalyst, 100 mg bagasse, 2.5 M NaOH in a mixed solution of DMSO and water (V:V=1:1), light reaction for 4 h. Detection at different wavelengths with Evaporative Light-scattering Detector (ELSD).

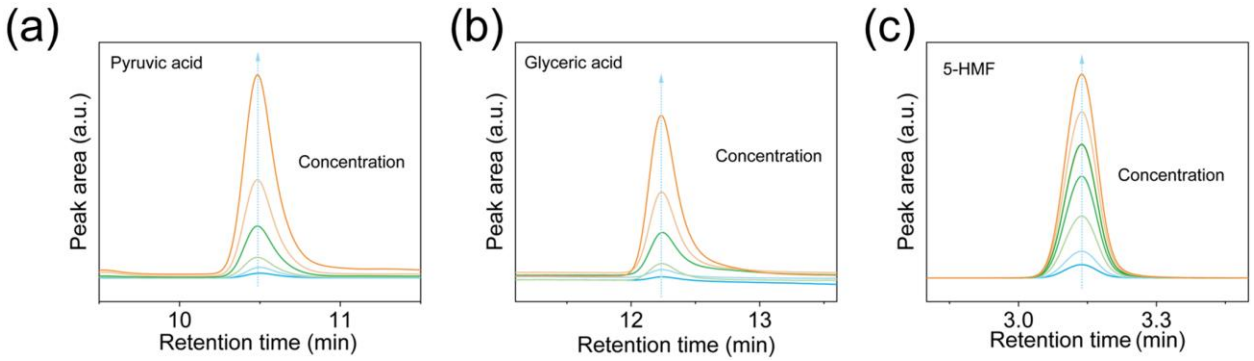

Fig. S12. Response plots of organic acid and 5-HMF standards on an VWD.

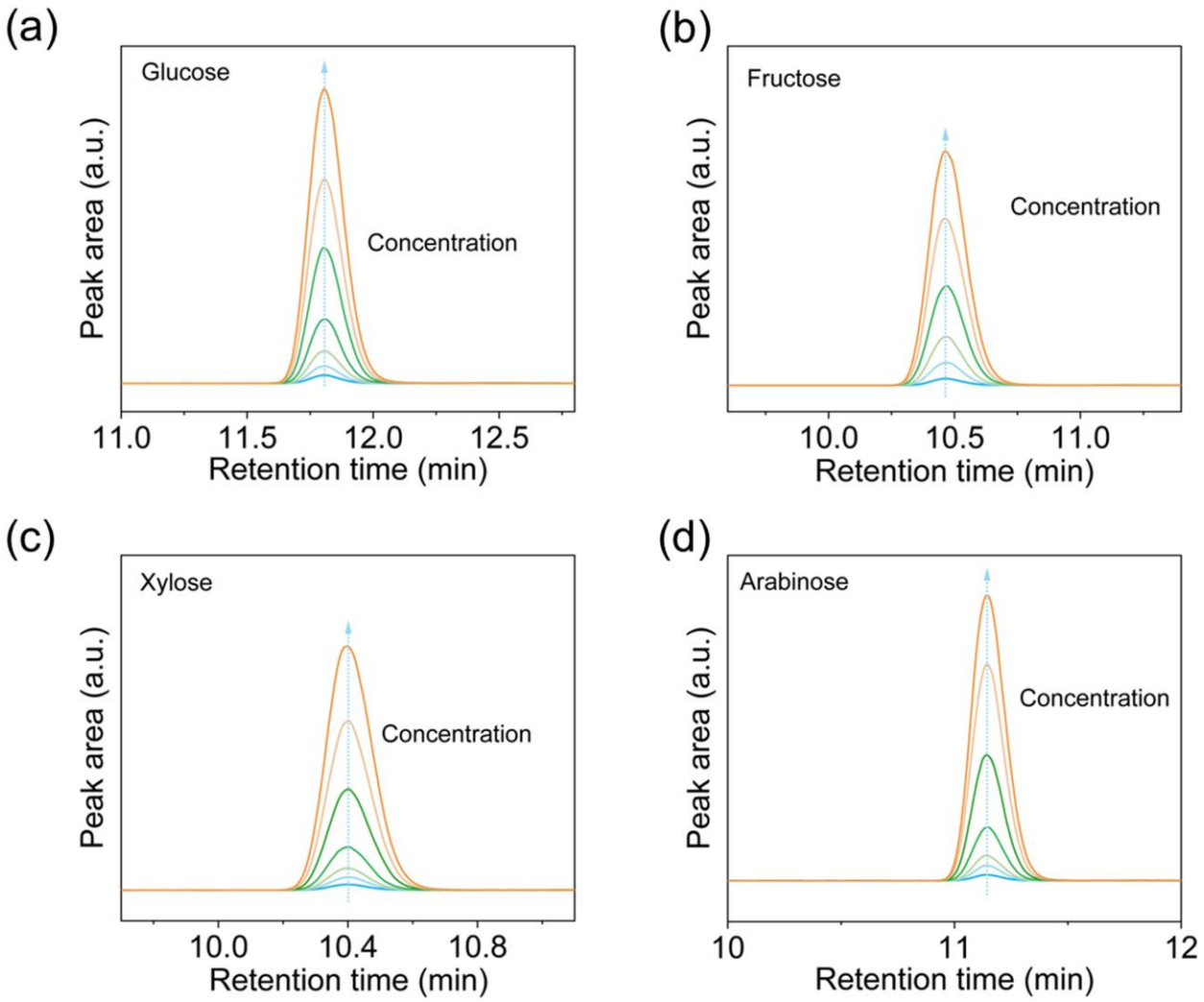

Fig. S13. Response plots of sugar standards on an ELSD.

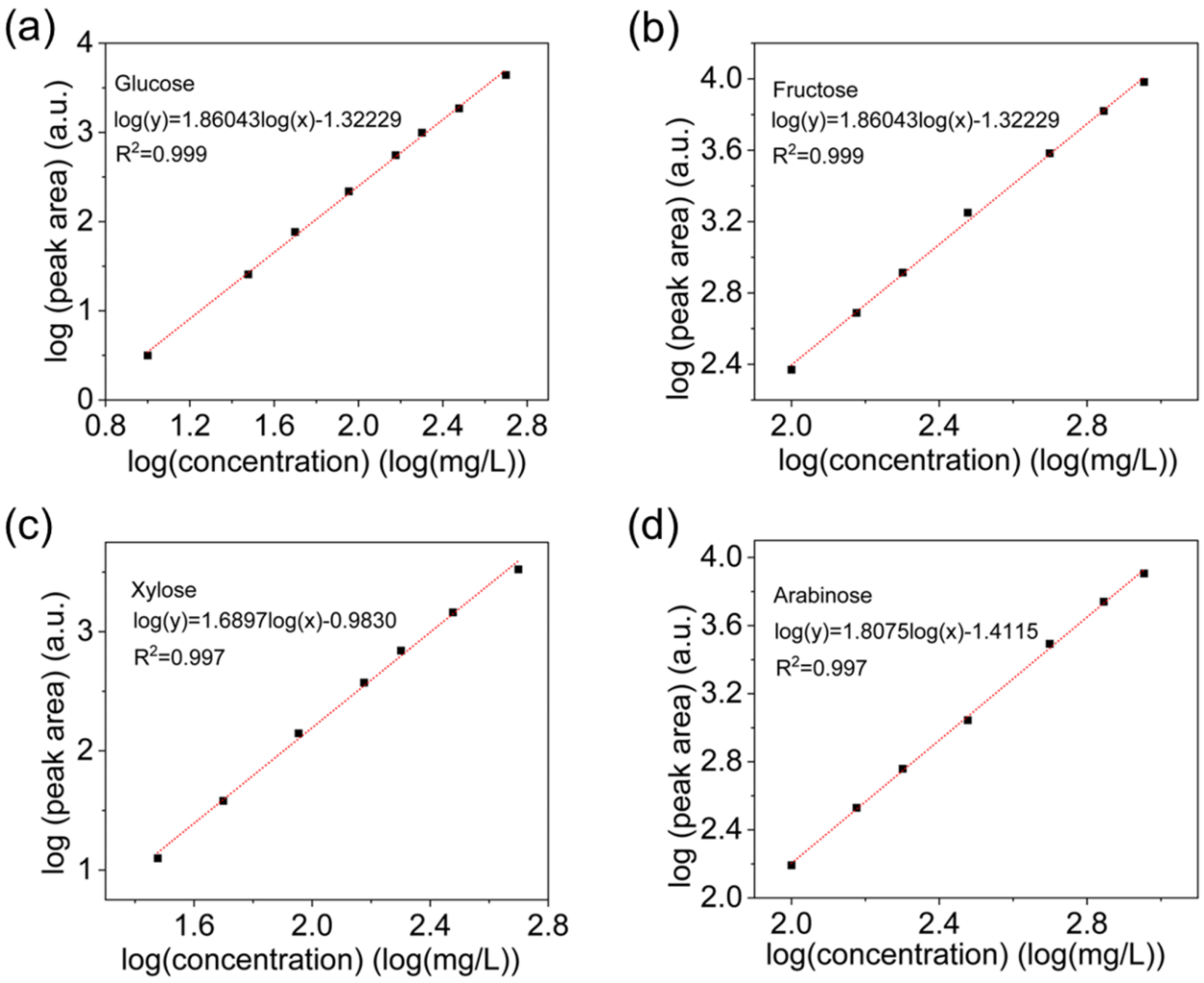

Fig. S14. Liquid chromatographic standard curves for sugars. The logarithmic fitting method was used for fitting (x: standard sample concentration (mg/L; y: the chromatographic peak area)). Sugar detection was performed at different wavelengths with VWD.

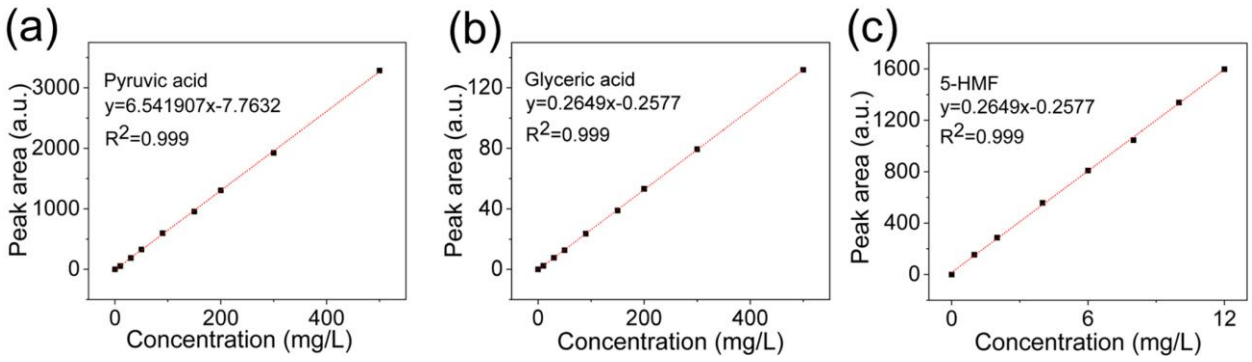

Fig. S15. Liquid chromatographic standard curves for organic acids and 5-HMF. Analyzed using linear fitting methods (x: standard sample concentration (mg/L; y: the chromatographic peak area). Organic acids and 5-HMF detection was performed using an ELSD.

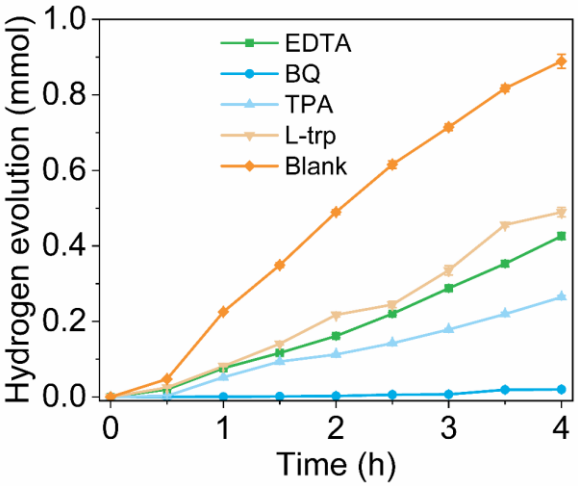

Fig. S16. Raw biomass photorefining freed radical trapping experiments in the hydrogen production. Hydrogen evolution properties in free radical trapping experiments. Photorefining reaction conditions: 100 mg bagasse, 25 mg catalyst, DMSO:water = 25 mL: 25 mL, 5 g NaOH, reaction time: 4 h and 300 W xenon lamp as the light source (scavenger agent is variable).

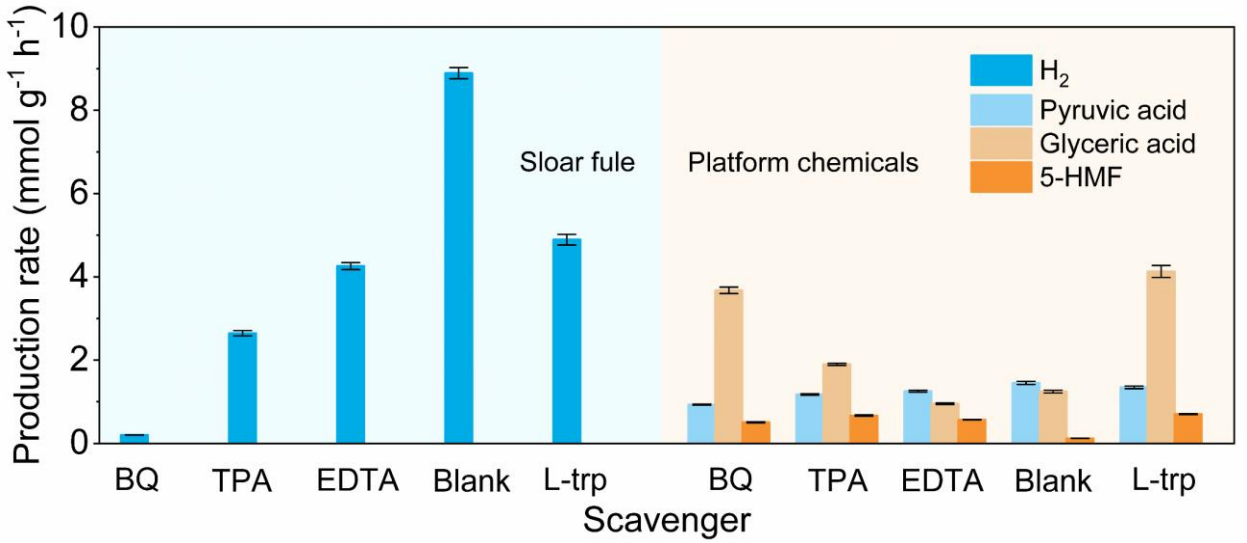

Fig. S17. Raw biomass photorefining bifunctional performance testing of composites for freed radical trapping experiments. The photorefining rate of free radical burst experiments. Photorefining reaction conditions: 100 mg bagasse, 25 mg catalyst, DMSO:water = 25 mL: 25 mL, 5 g NaOH, reaction time: 4 h and 300 W xenon lamp as the light source (scavenger agent is variable).

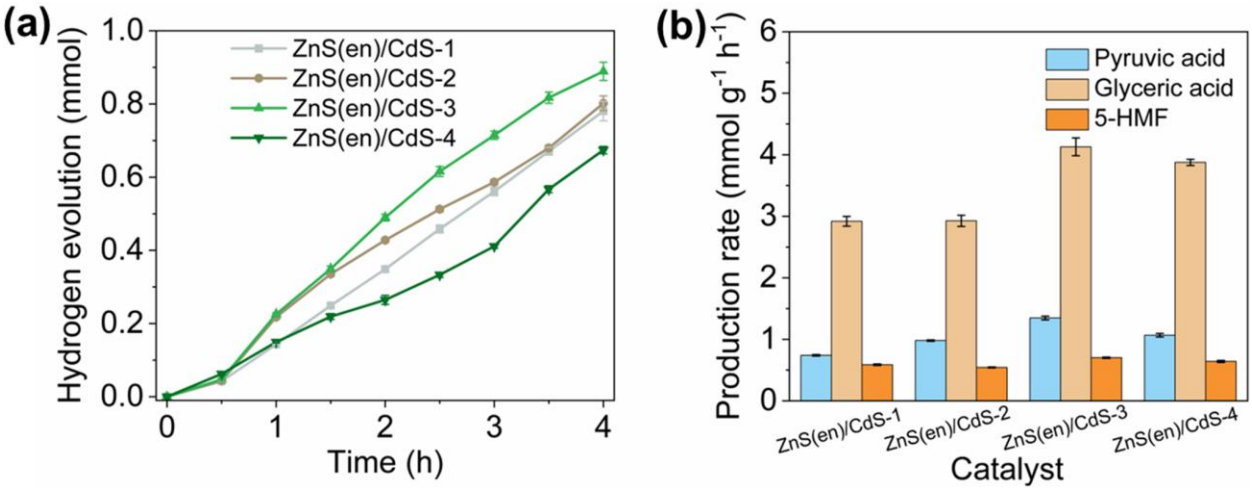

Fig. S18. Effect of catalyst ratio on bifunctional performance of raw biomass photorefining. (a)-(b) Effect of catalyst ratio for raw biomass photorefining. Photorefining reaction conditions: 100 mg bagasse, 25 mg catalyst, DMSO:water = 25 mL: 25 mL, 5 g NaOH, reaction time: 4 h and 300 W xenon lamp as the light source (catalyst is variable).

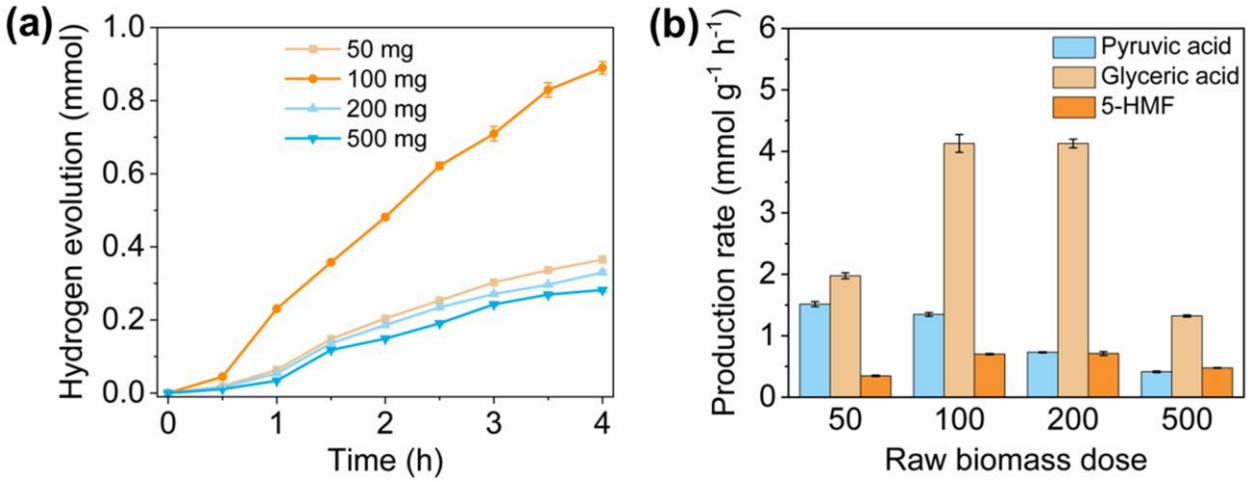

Fig. S19. Influence of the amount of raw biomass on the photorefining process. (a)-(b) Effect of substrate amount on the photorefining reaction. Photorefining reaction conditions: bagasse, 25 mg catalyst, DMSO:water = 25 mL: 25 mL, 5 g NaOH, reaction time: 4 h and 300 W xenon lamp as the light source (bagasse is variable).

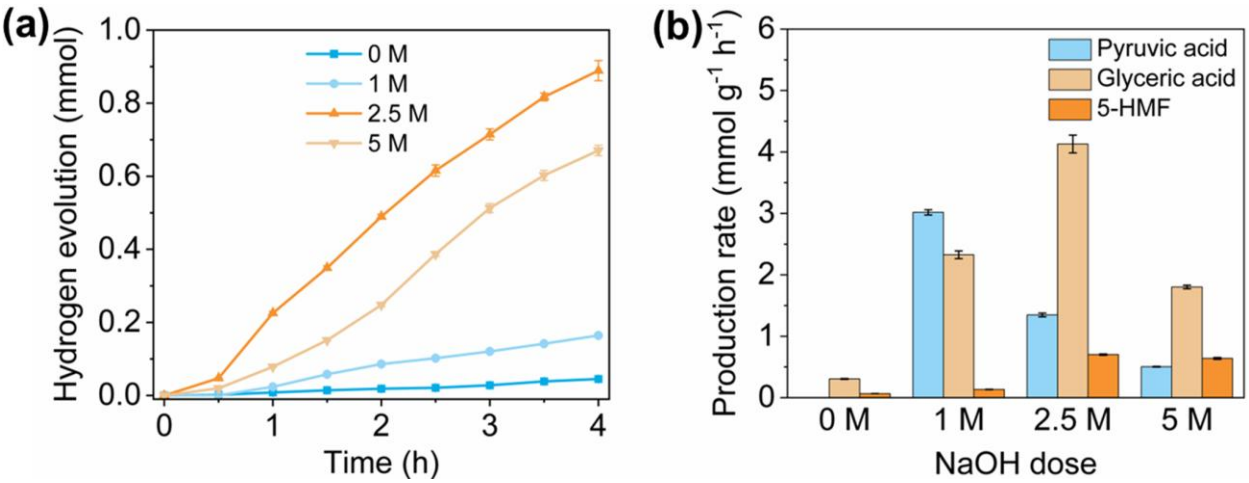

Fig. S20. Effect of alkali dosage on solar-driven refining raw biomass conversion in the catalytic system. (a)-(b) Effect of alkali concentration on the reaction. Photorefining reaction conditions: 100 mg bagasse, 25 mg catalyst, DMSO:water = 25 mL: 25 mL, NaOH, reaction time: 4 h and 300 W xenon lamp as the light source (NaOH is variable).

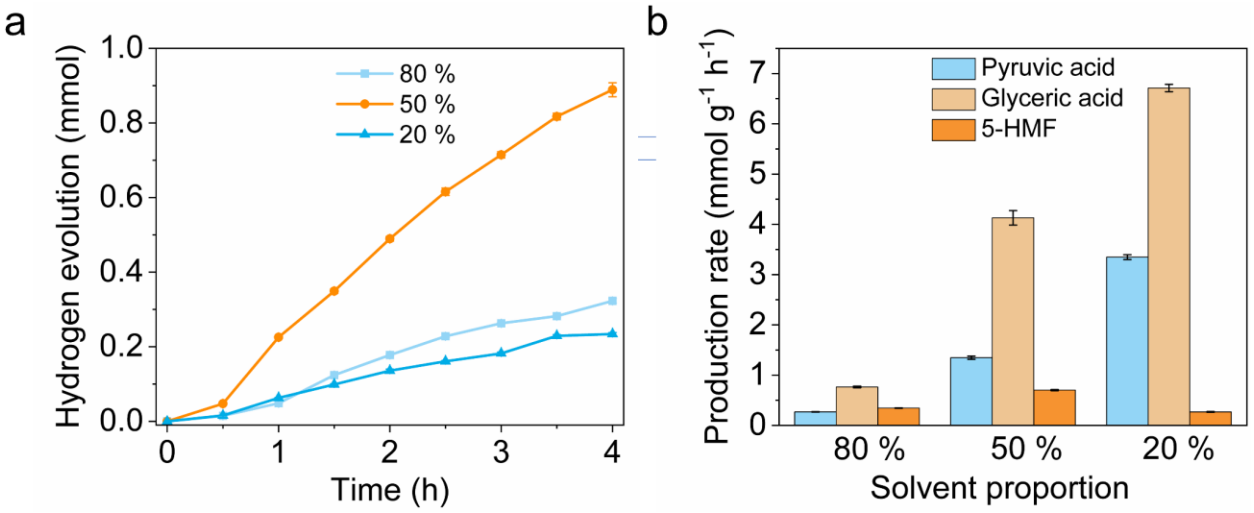

Fig. S21. Effect of solvent ratio on the bifunctional properties of photorefining. (a)-(b) Effect of solvent ratio on reaction (Water content 80 %, 50 %, and 20 % respectively). Photorefining reaction conditions: 100 mg bagasse, 25 mg catalyst, DMSO:water, 5 g NaOH, reaction time: 4 h and 300 W xenon lamp as the light source (solvent proportion is variable, total volume of the solvent: 50 mL).

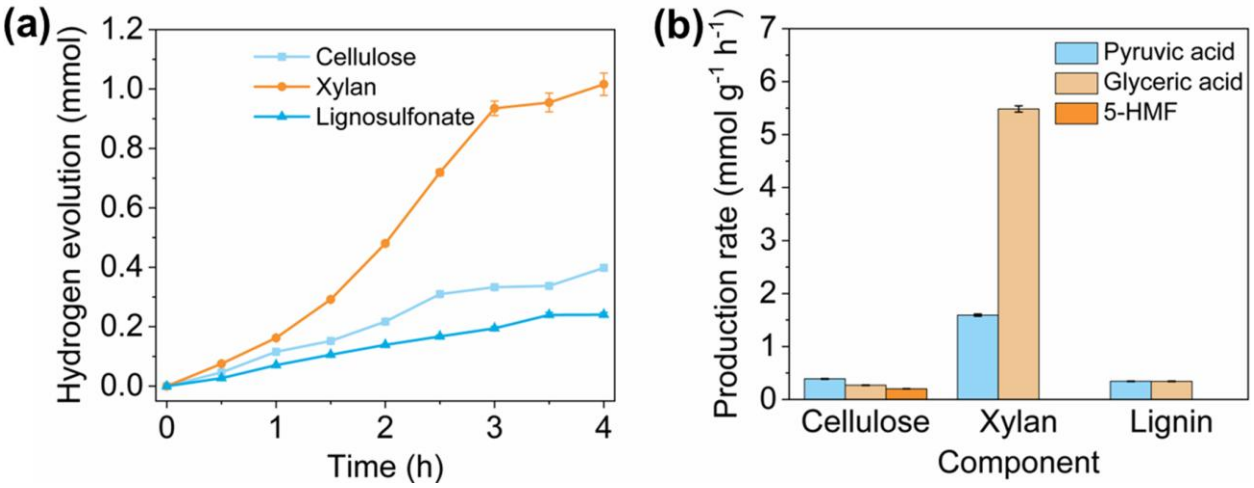

Fig. S22. An investigation into the photorefining process of the main component of lignocellulose. (a)-(b) Photorefining effect on the three main components of lignocellulose. Photorefining reaction conditions: 100 mg substrate, 25 mg catalyst, DMSO:water, 5 g NaOH, reaction time: 4 h and 300 W xenon lamp as the light source (substrate is variable).

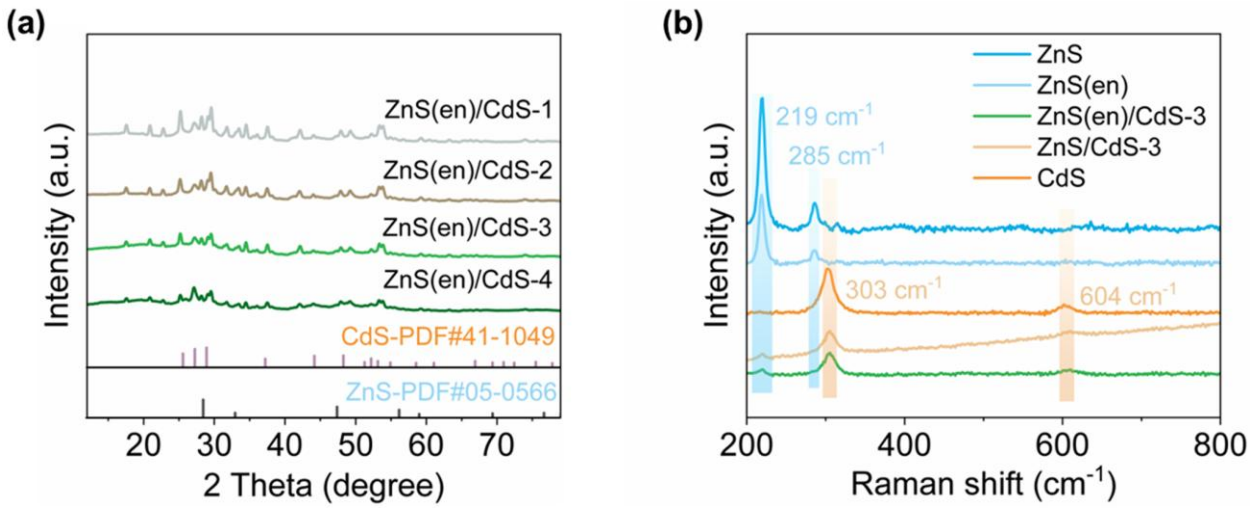

Fig. S23. Microstructure analysis of materials. (a) XRD pattern and Raman spectrum (b) of ZnS(en)/CdS-3.

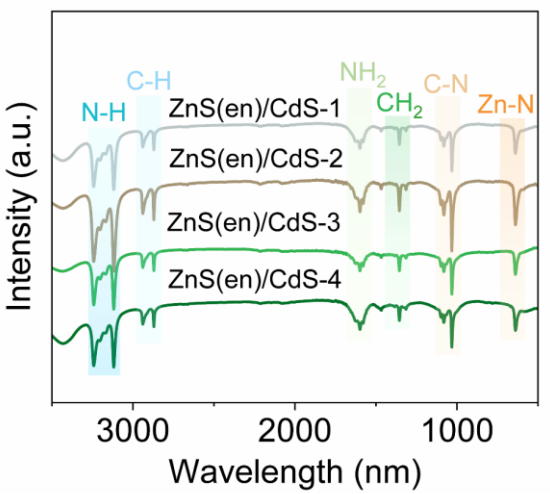

Fig. S24. Surface chemical functional group analysis of catalysts. FT-IR spectra of ZnS(en)/CdS.

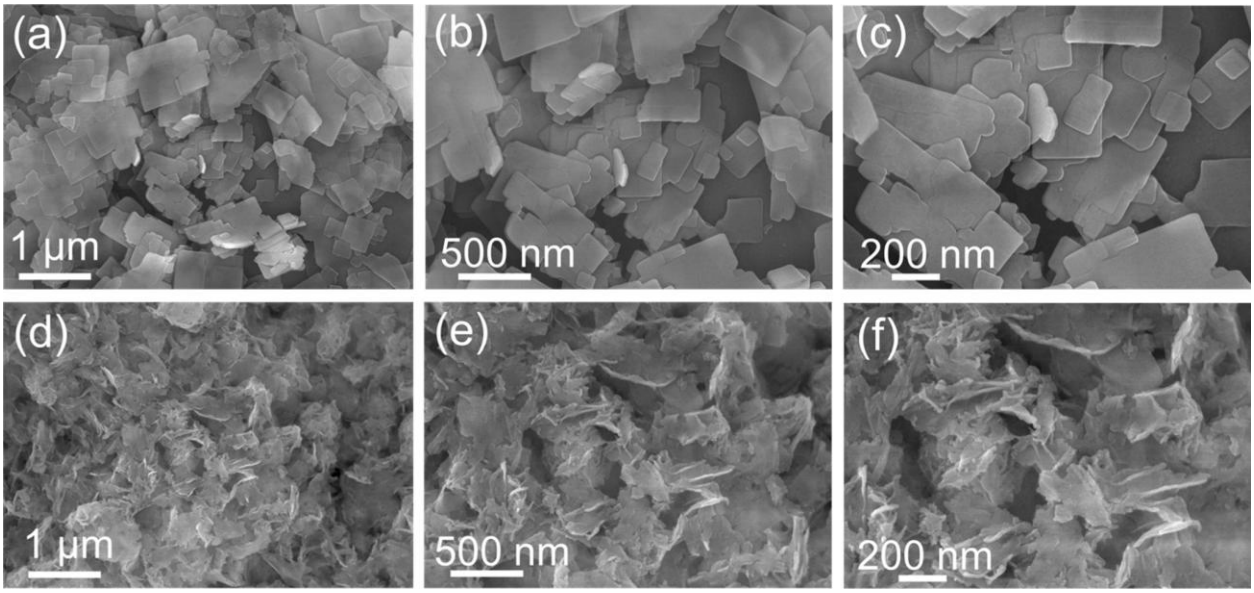

Fig. S25. Morphological characterization of single materials.(a)-(c) F-SEM images of ZnS(en) and CdS (d)-(f).

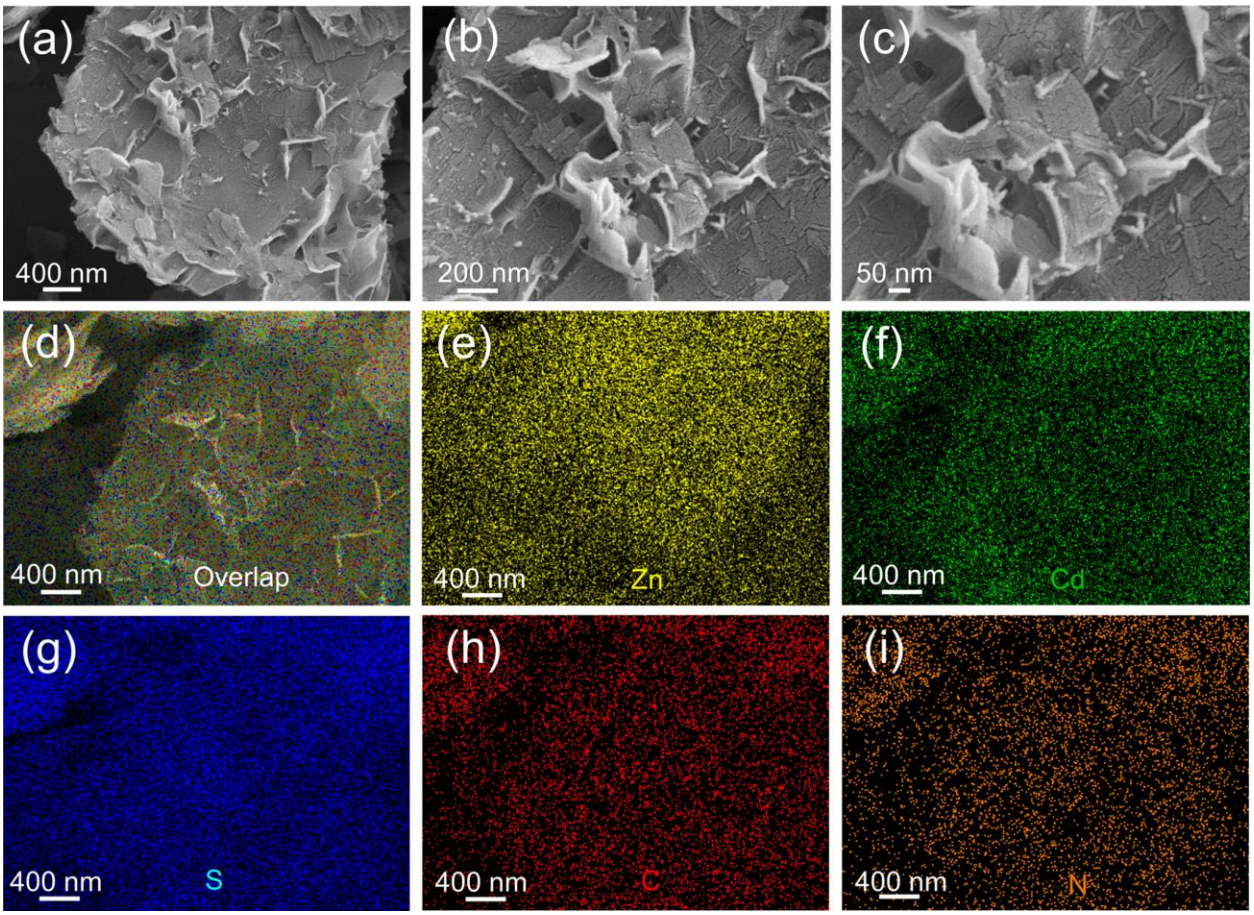

Fig. S26. Analysis of morphology and surface element distribution of composite materials. (a)-(c) SEM images of ZnS(en)/CdS-3. (d)-(i) EDS elemental mapping of ZnS(en)/CdS-3.

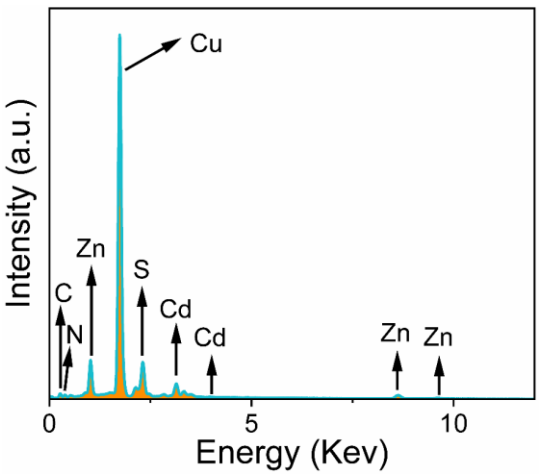

Fig. S27. Exploration of surface element content of composite materials. SEM-EDS spectra of ZnS(en)/CdS-3.

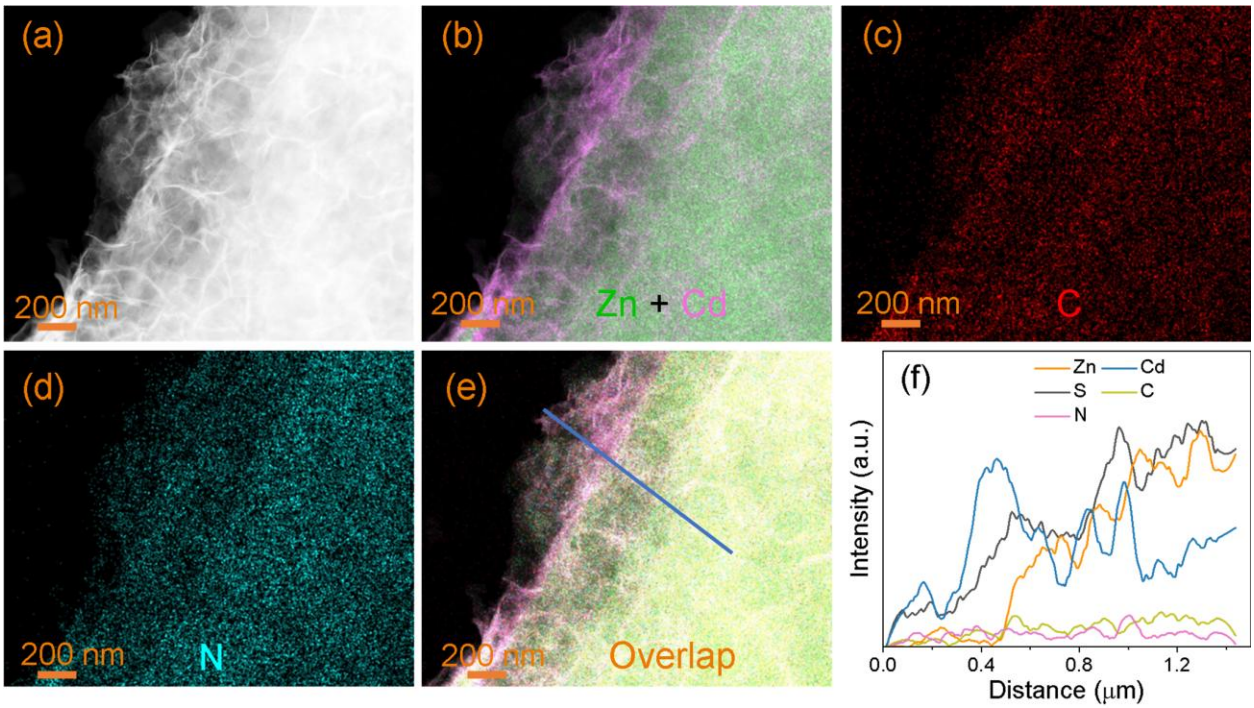

Fig. S28. Spatial distribution and elemental content variation at material interfaces. (a)-(e) EDS elemental mapping of ZnS(en)/CdS-3. (f) Element line scanning distribution of ZnS(en)/CdS-3.

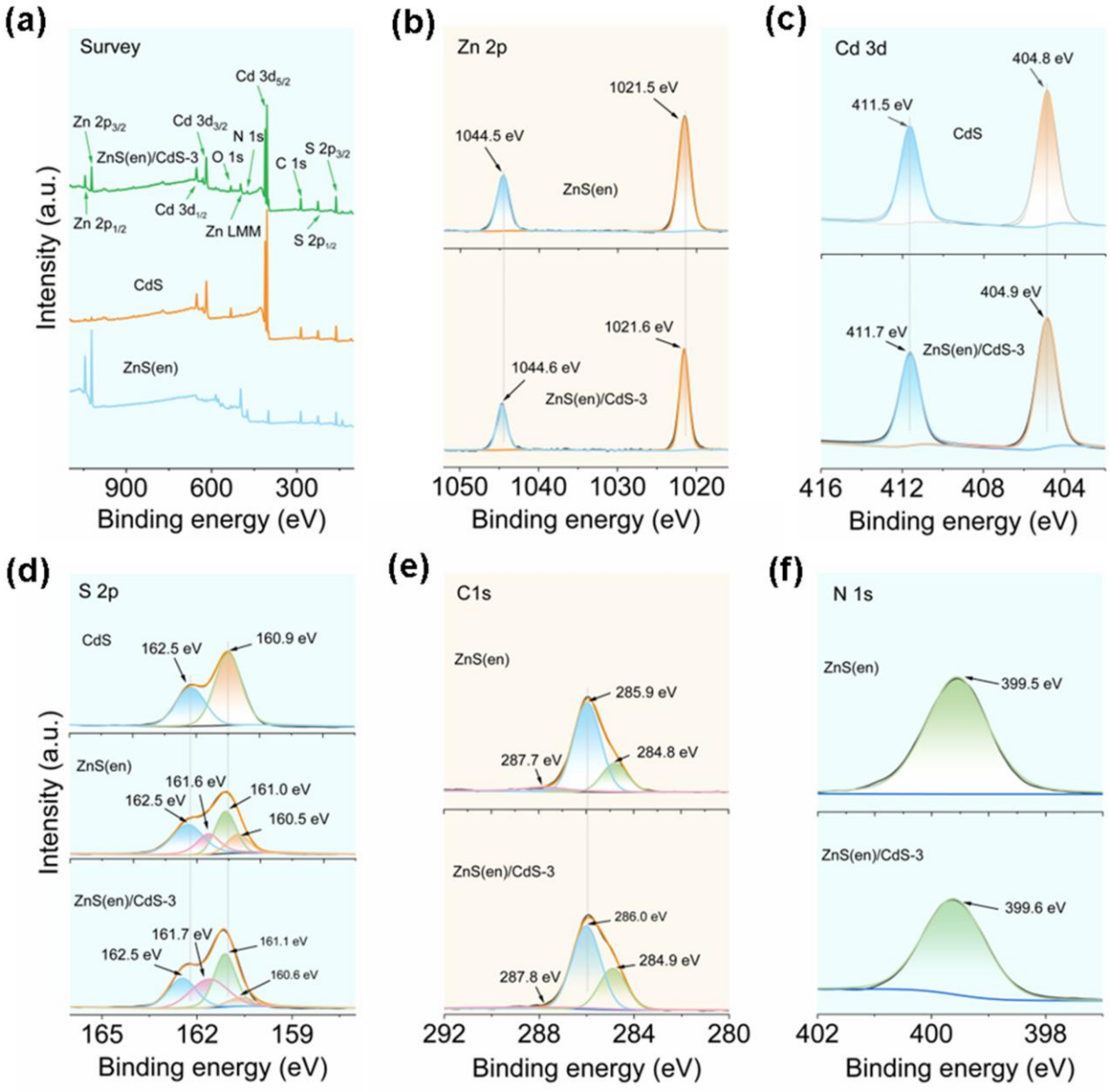

Fig. S29. Elemental chemical state analysis of materials. (a) XPS survey spectra. (b)-(f) XPS fine spectra Zn 2p, Cd 3d, S 2p, C 1s and N 1s.

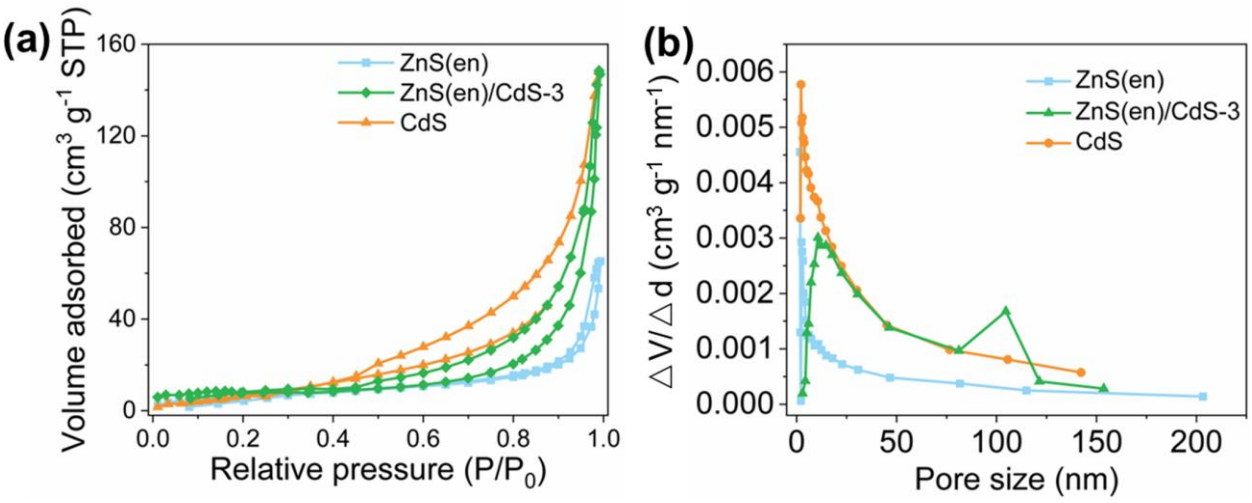

Fig. S30. Characterization of specific surface area and pore size distribution of catalysts. (a) N_2 adsorption-desorption isotherms. (b) Pore size distribution of the material.

Table S2 BET surface parameters of ZnS(en)/CdS samples.

Samples	Surface parameters		
	BET surface area (m^2 g^{-1})	Pore volume (cm^3 g^{-1})	Pore diameter (nm)
ZnS(en)	22.482	0.043	16.413
CdS	35.283	0.119	11.959
ZnS(en)/CdS-3	24.098	0.094	19.581

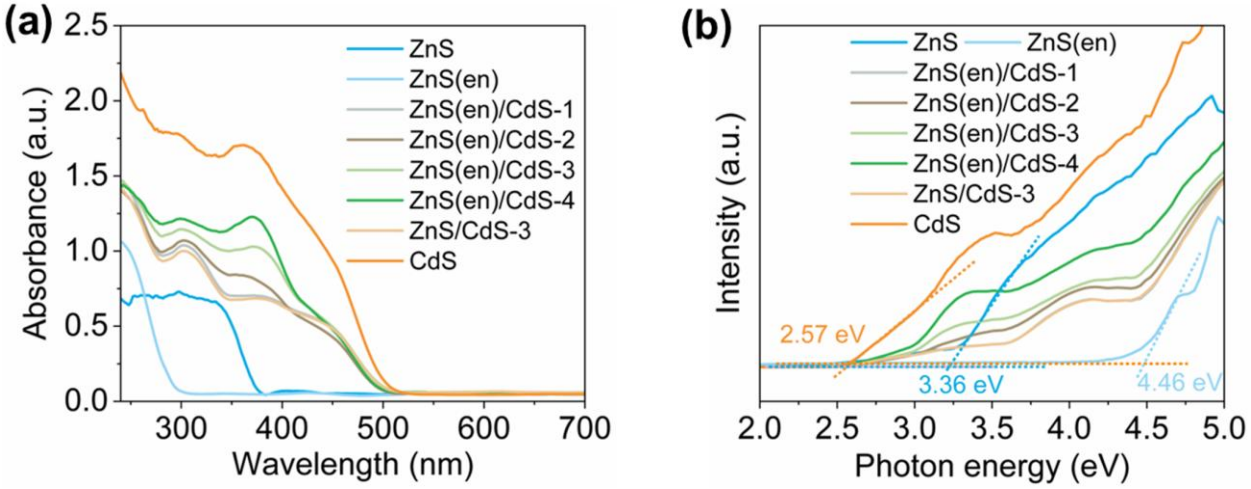

Fig. S31. Exploration of light absorption properties and band gap structure of materials. (a) Uv-vis DRS spectra. (b) Tauc plots of ZnS(en)/CdS.

Table S3 Band gap structures and photogenerated charges average lifetimes of ZnS(en) and CdS.

Samples	E_g (eV)	E_{CB} (eV)	E_{VB} (eV)
ZnS(en)	4.46	-1.26	+3.20
CdS	2.57	-0.71	+1.86

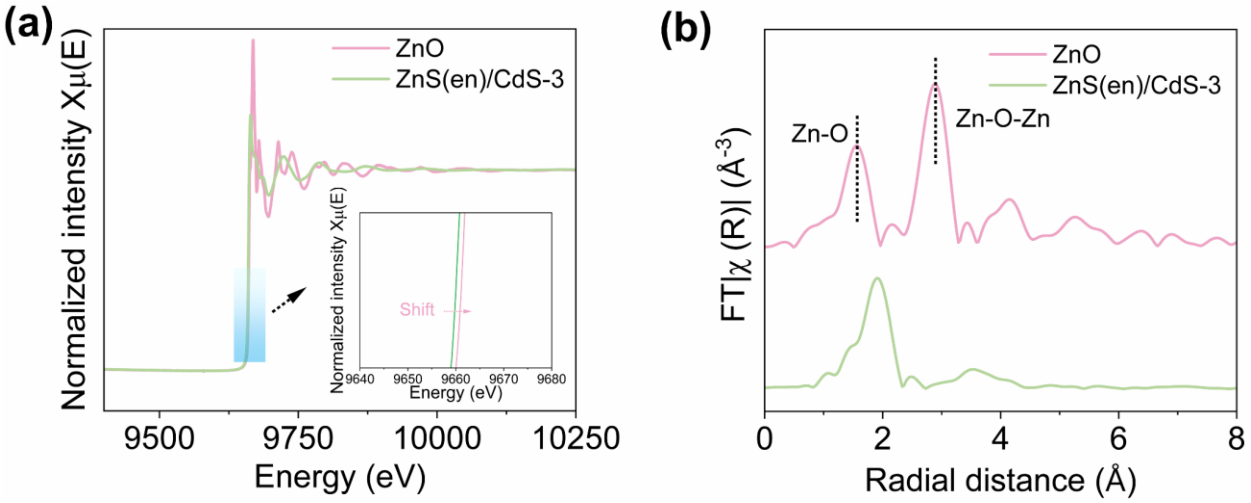

Fig. S32. Analysis of x-ray absorption near-edge structure and associated chemical bonds. (a)-(b) Zn K-edge XANES spectra of ZnO and ZnS(en)/CdS-3.

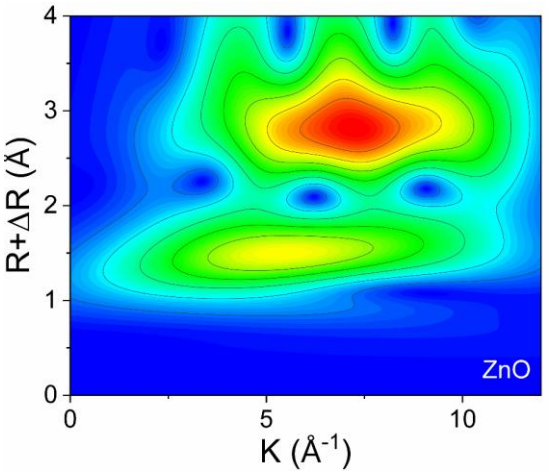

Fig. S33. Wavelet transformed 2D plan map of ZnO. Wavelet transform of k^3-weighted EXAFS spectra of ZnO.

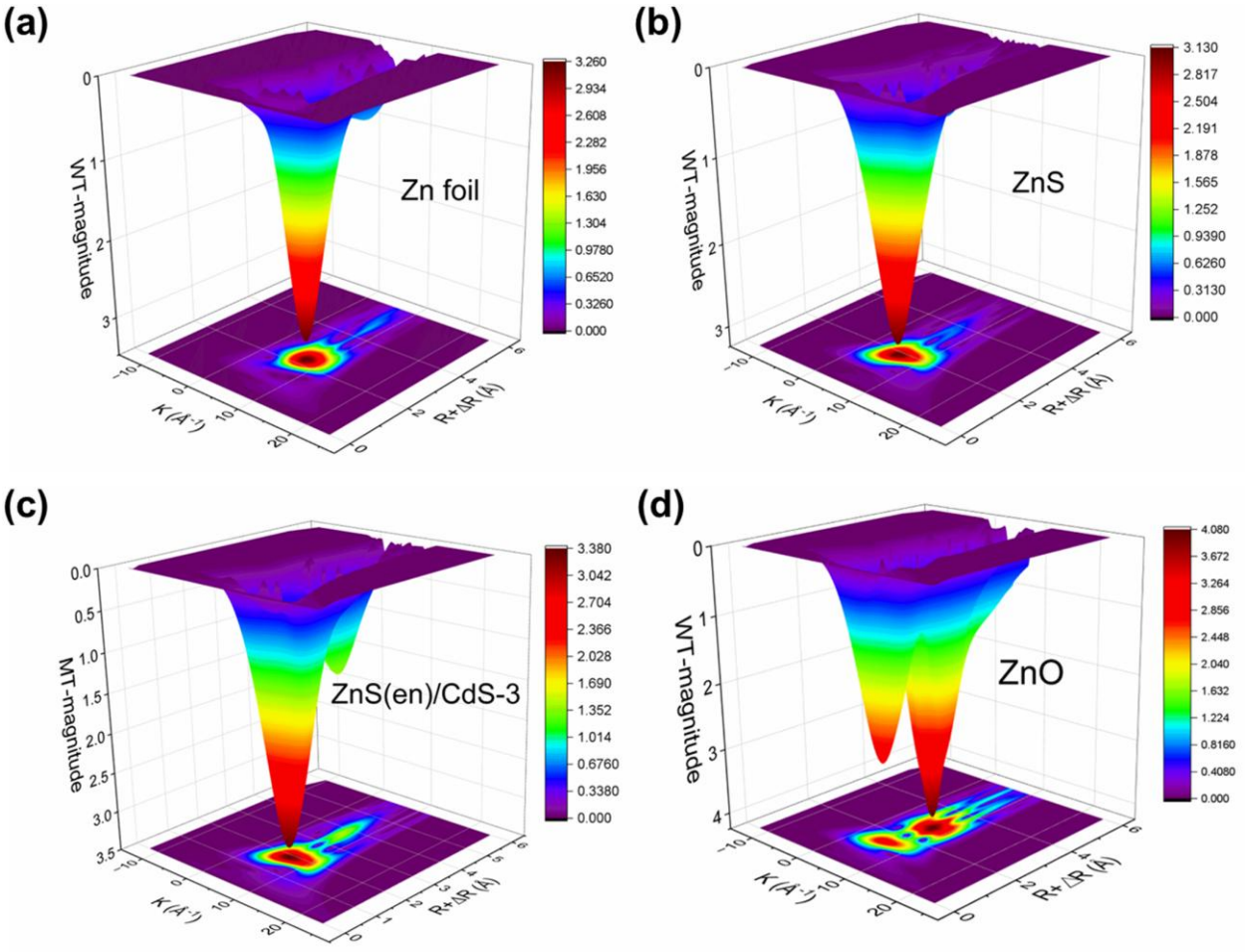

Fig. S34. 3D wavelet transform plots of materials and standard samples. (a)-(d) Wavelet transform of k^3-weighted EXAFS spectra of Zn foil, ZnS, ZnS(en)/CdS-3 and ZnO in the three-dimensional space.

Table S4 EXAFS fitting parameters at the Zn K-edge for various samples (S_0^2=0.875).

Sample	Shell	[a]CN	[b]R(Å)	[c]σ^2 (Å$^2\cdot10^{-3}$)	[d]ΔE_0(eV)	R factor (%)
ZnS(en)/CdS-3 sample	Zn-N	1.08±0.22	2.15±0.05	0.003	7.67±0.88	0.94
	Zn-S	3.55±0.58	2.36±0.01	0.004±0.002		

[a]CN, coordination number; [b]R, distance between absorber and backscatter atoms; [c]σ^2, Debye-Waller factor to account for both thermal and structural disorders; [d]ΔE_0, inner potential correction; R factor indicates the goodness of the fit. Fitting range: 2.0 < k (/Å) < 10.0 and 1.0 < R (Å)< 3.0.

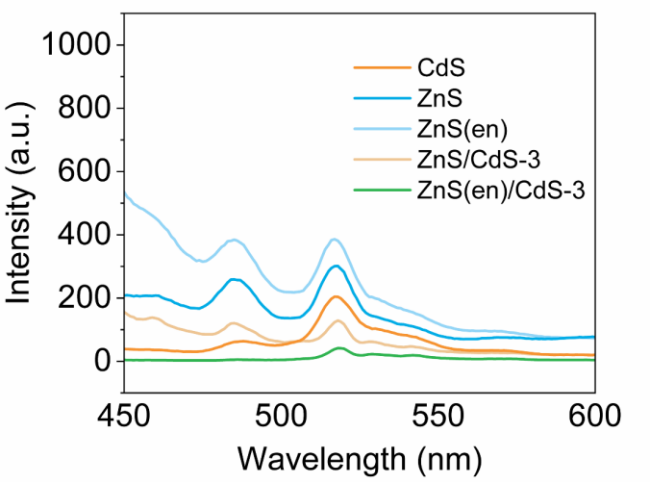

Fig. S35. Carrier recombination exploration of photogenerated carrier dynamics. Photoluminescence spectrum of ZnS(en)/CdS.

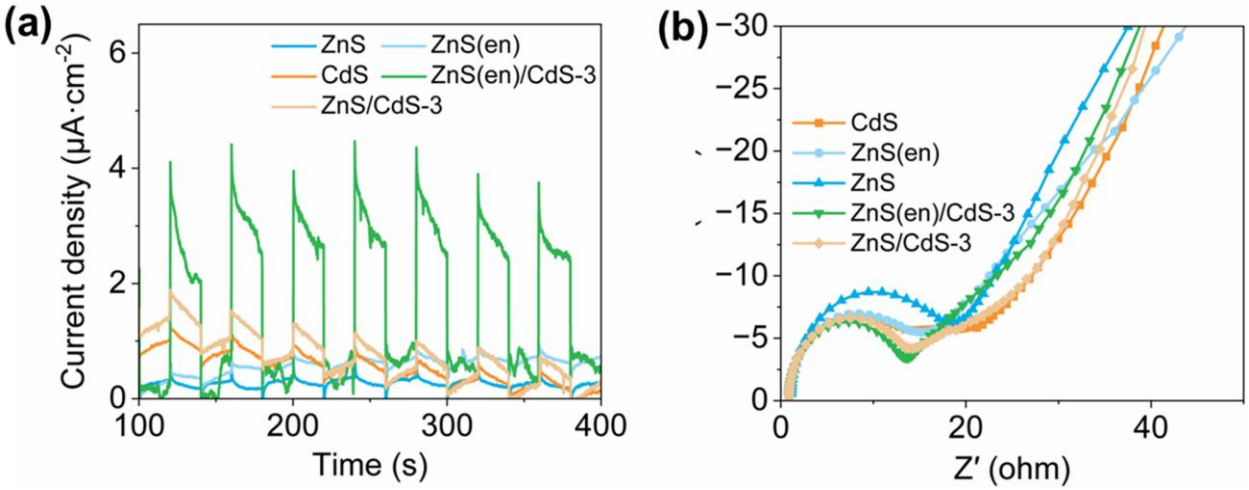

Fig. S36. Analysis of photocurrent density and interfacial resistance of materials. (a) Transient photocurrent response. (b) Electrochemical impedance spectroscopy (EIS) Nyquist plots.

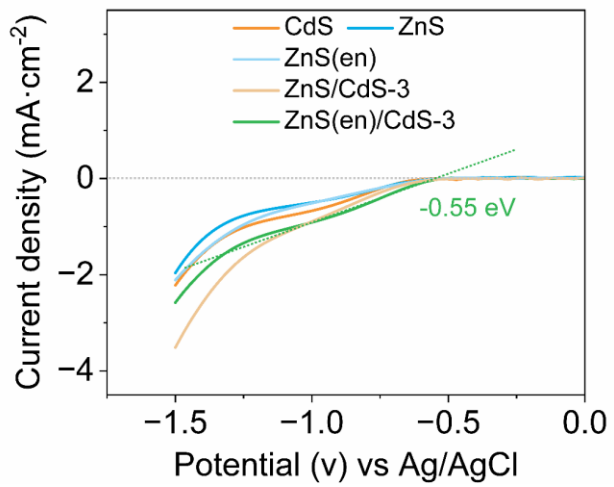

Fig. S37. Hydrogen production potential testing of materials and interface overpotential analysis. Linear sweep voltammetry (LSV) curves.

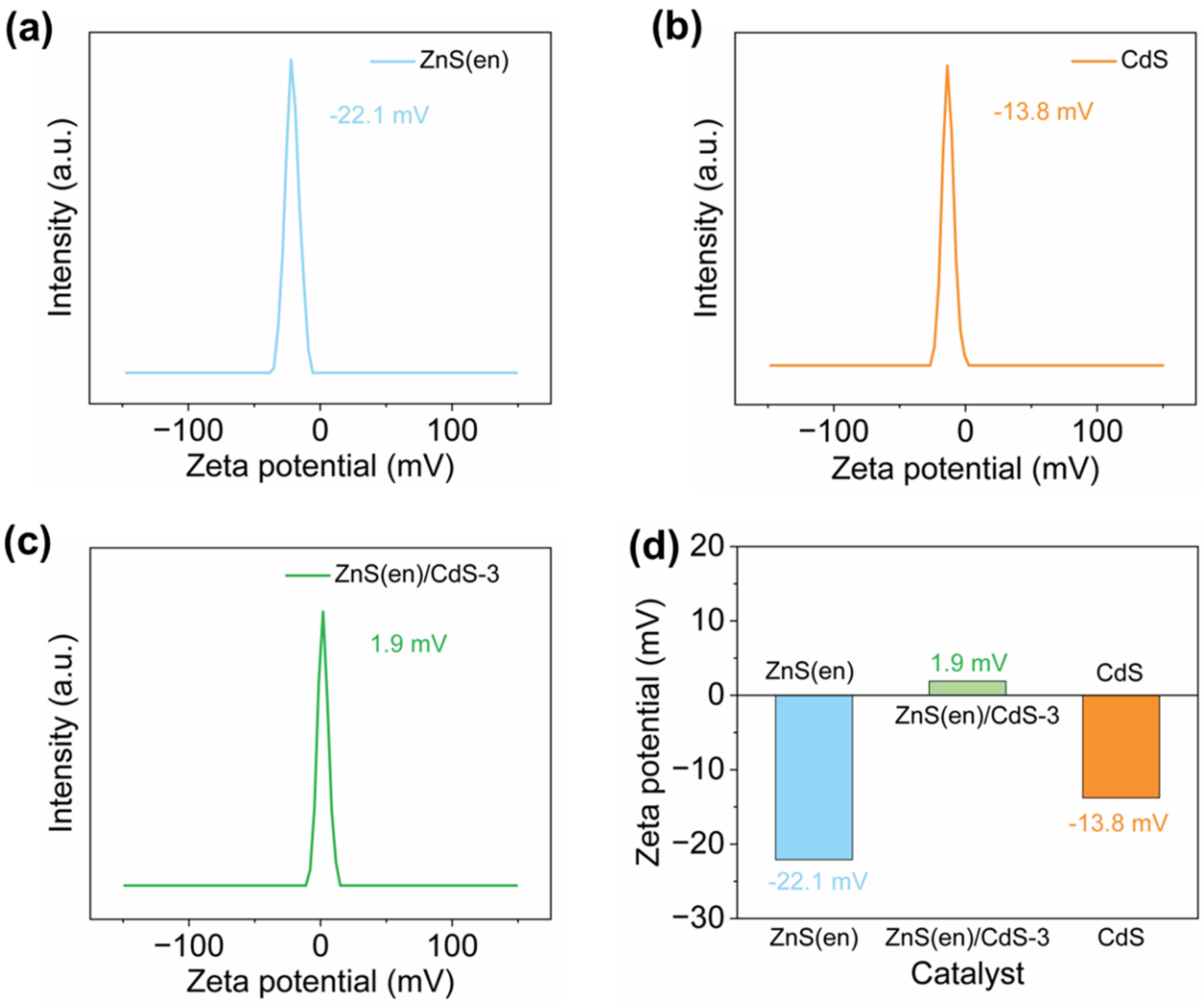

Fig. S38. Investigation of surface potential changes in catalysts. (a)-(c) Zeta potential of ZnS, CdS and ZnS(en)/CdS-3. (d) Comparison image.

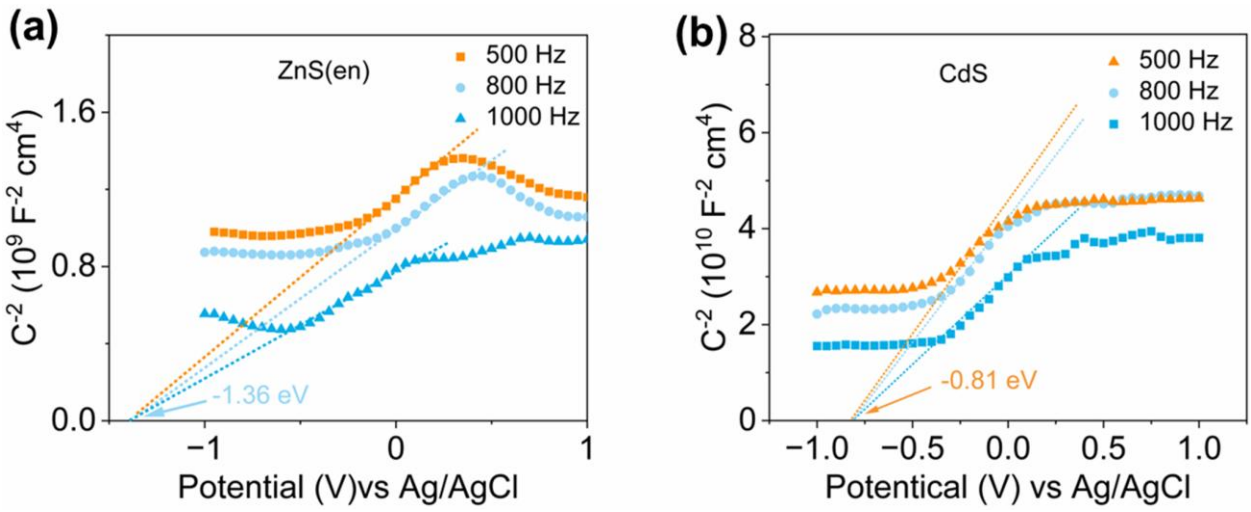

Fig. S39. Flat charge potential test for materials. (a)-(b) Mott-Schottky (M-S) plots.

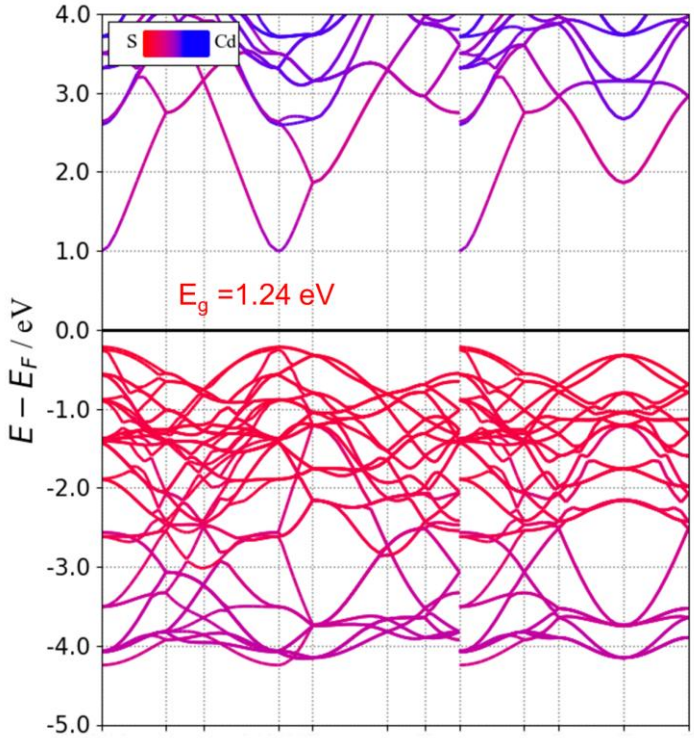

Fig. S40. Theoretical simulation of band gap structure of CdS materials. Theoretically calculated bandgap structure of CdS.

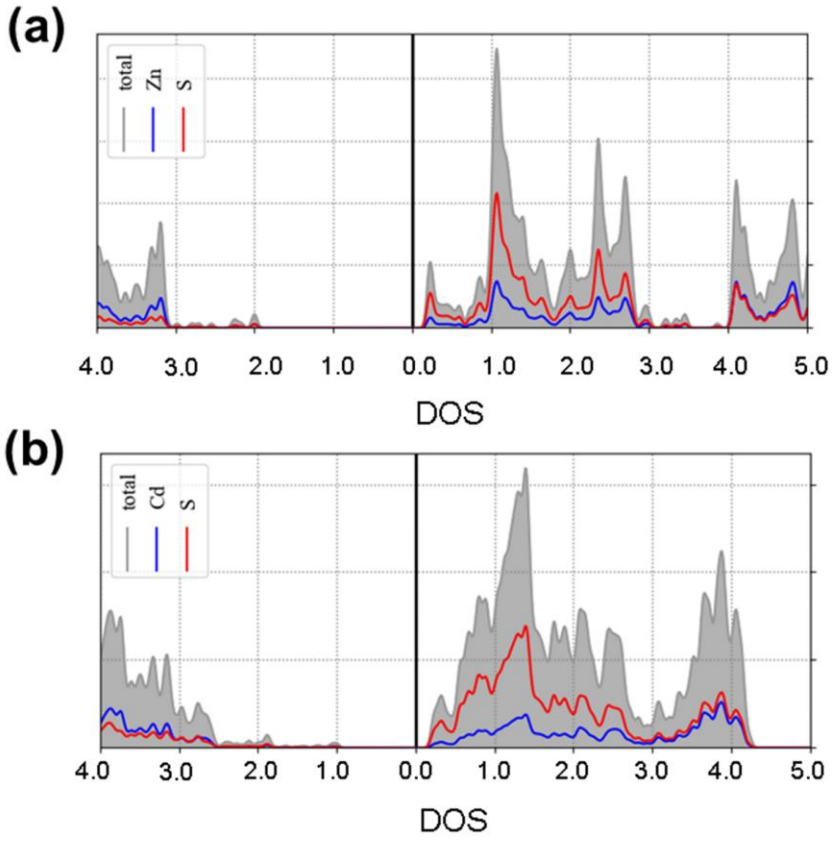

Fig. S41. The density of state (DOS) simulation of materials. (a)-(b) The DOS of ZnS and CdS.

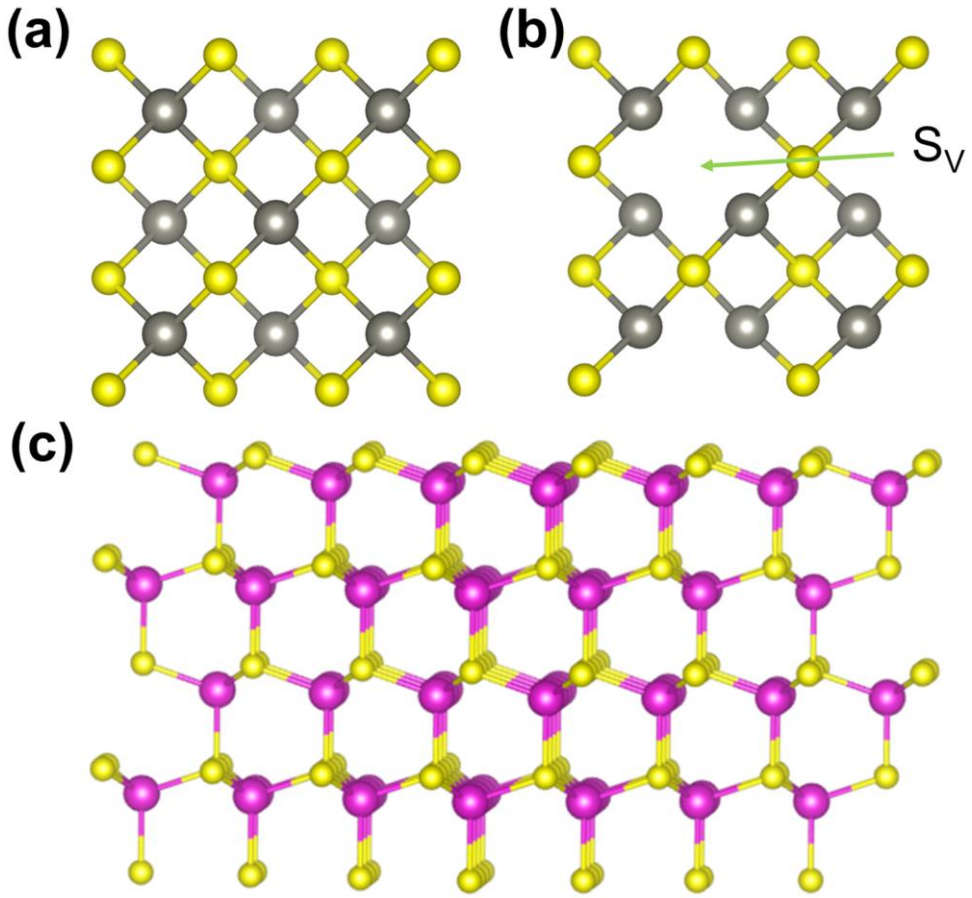

Fig. S42. Structural modeling of materials in theoretical calculations. (a)-(c) Theoretical model of ZnS, ZnS(S_V), CdS.

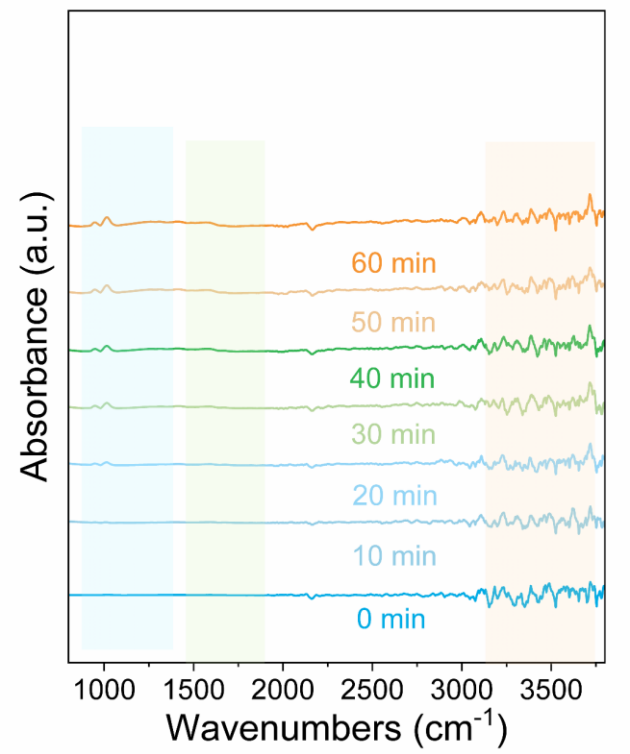

Fig. S43. Functional group and chemical bonding changes for raw biomass photorefining in platform compound generation. In situ FT-IR spectrum (800-3600 cm^{-1}) of ZnS(en)/CdS.

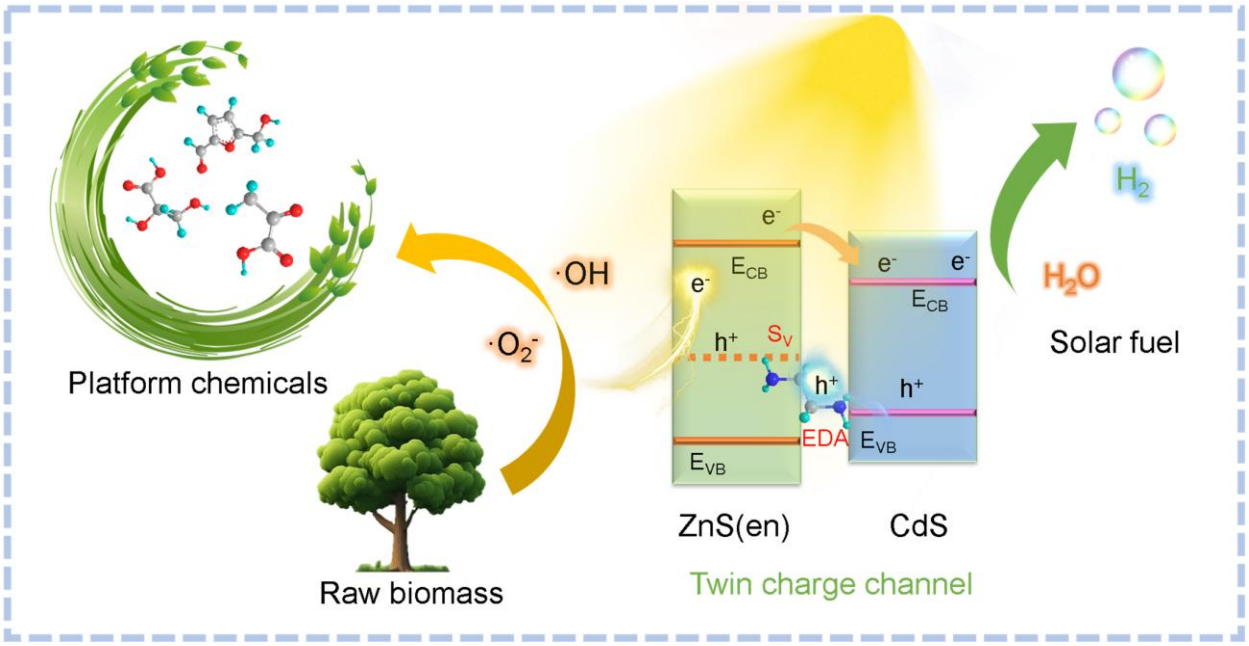

Fig. S44. Catalyst interfacial charge transition and migration in sunlight-driven raw biomass conversion. Carrier migration at the ZnS(en)/CdS-3 interface.

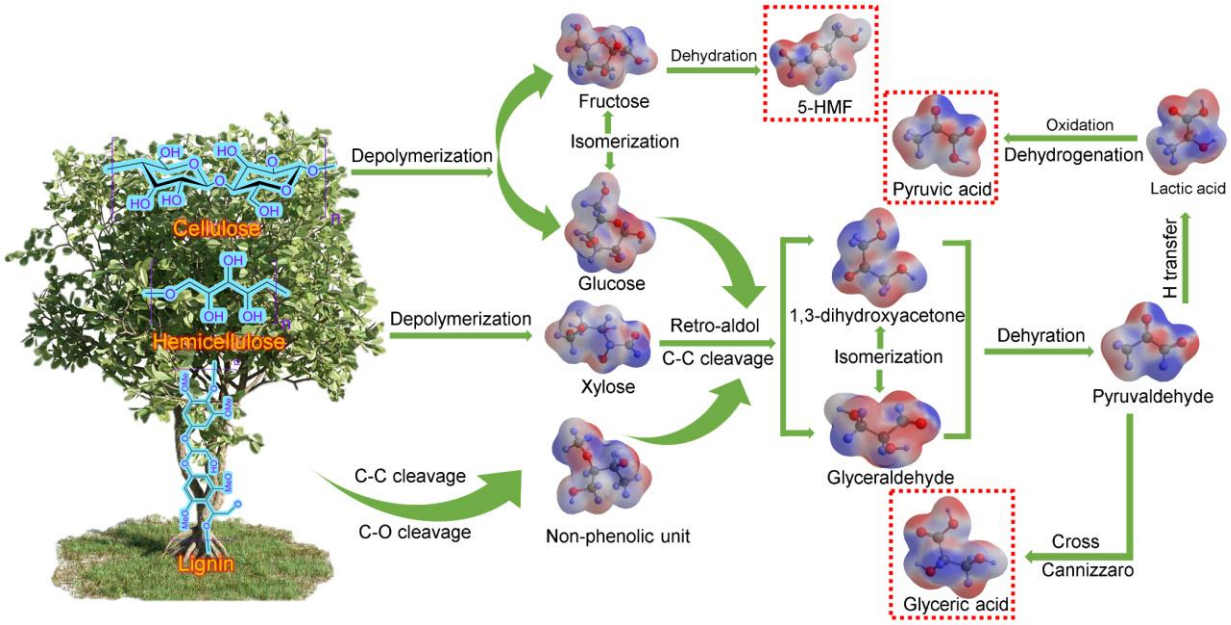

Fig. S45. Conversion of raw biomass to platform compounds. Raw biomass conversion pathway (ball-and-stick model).

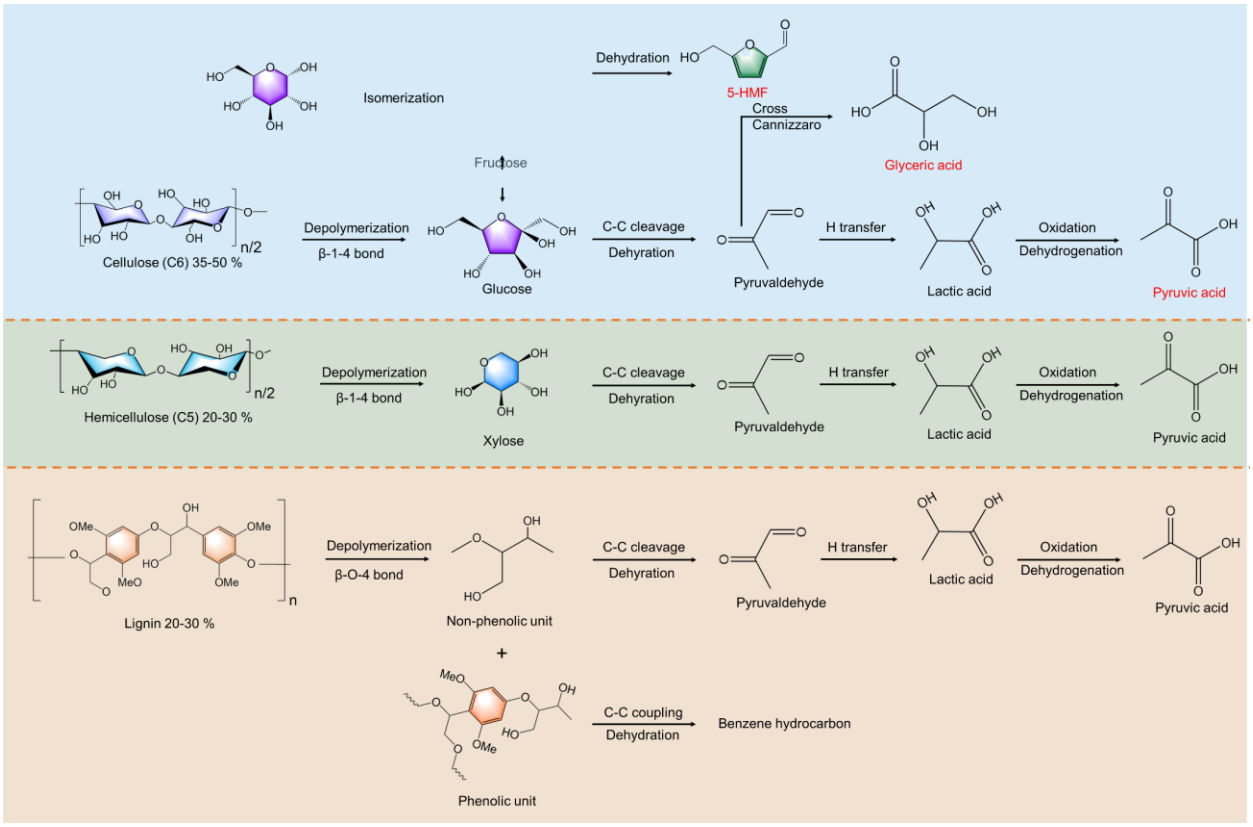

Fig. S46. Conversion pathways for the main components of raw biomass. Conversion pathways of lignocellulose main components (molecular formula).

$ZnS(en)/CdS+hv \rightarrow e^{-}+h^{+}$ (S1)

$ZnS(en)\ (e^{-}) \rightarrow CdS\ (e^{-})$ (S2)

$CdS(h^{+}) \rightarrow ZnS\ (h^{+})$ (S3)

$CdS\ (e^{-})+H^{+} \rightarrow H_2$ (sloar fuel) (S4)

$e^{-}+ O_2 \rightarrow \bullet O_2^{-}$ (S5)

$\bullet O_2^{-}+ H^{+}+ e^{-} \rightarrow \bullet OH+OH^{-}$ (S6)

$OH^{-}+ h^{+} \rightarrow \bullet OH$ (S7)

$\bullet OH$+raw biomass→platform compound (S8)

$\bullet O_2^{-}$+raw biomass→platform compound (S9)

Table S5 Comparison raw biomass photorefining of different catalysts on the generation of H_2 and platform compounds.

Catalysts	H_2 evolution rate (mmol h^{-1} g^{-1})	Substrate	Organic acid (mmol h^{-1} g^{-1})	Furfural class (mmol h^{-1} g^{-1})	Refs.
g-C_3N_4	0.08	poplar power			1
5 % Pt/TiO_2	0.10	cherry wood			2
MoS_2/$ZnIn_2S_4$	0.01	poplar wood chip			3
Pt (1 %)/P25TiO_2	0.21	pretreated corn stover			4
Pt_1Au_3/CN	0.41	wooden branch			5
ZnS-1198	0.07	wood			6
2 % Pt/$[SO_4]^-$$ZnIn_2S_4$(0.5)	0.18	wood chip			7
Ag_xPt_{4x}/CN	0.19	cedar tree branch			8
1 % MoS_2@TiO_2	0.05	corncob			9
MoS_2/VS-$ZnIn_2S_4$	0.13	bamboo			10
0.2 wt % Pt/TiO_2	1.23	willow			11
Co/CdS/CdO_x	5.31	wooden branch			12
ZnS(en)/CdS	8.89	bagasse	PA1.35; GA 4.13[a]	0.70	This work

[a]Pyruvic acid (PA), glyceric acid (GA)

Table S6 Comparison biomass photorefining of different catalysts on the generation of H_2 and platform compounds.

Catalysts	H_2 evolution rate (mmol h^{-1} g^{-1})	Substrate	Organic acid (mmol h^{-1} g^{-1})	Furfural class (mmol h^{-1} g^{-1})	Refs.
TiO_2	0.28	α-cellulose			13
CoO/g-C_3N_4	0.18	phosphoric acid swollen cellulose			14
carbon dots	0.27	α-cellulose			15
CN_x|Ni_2P	0.04	cellulose			16
MoS_2/TiO_2	0.20	α-cellulose			17
$^{HCN}CN_x$	0.19	cellulose dissolution solution			18
$^{HCN}CN_x$|Ni_2P	1.70	α-cellulose			19
CdO_x/CdS/SiC	0.36	cellulose			20
$CoTiO_3$-$[Co(bpy)_3]^{3+}$/$[Co(bpy)_3]^{2+}$–Pt/CdS	0.11	α-cellulose			21
h-ZnSe/Pt@TiO_2	1.86	cellulose	formic acid 0.37		22
CdZnS	5.51	waste straw			23
g-C_3N_4–C_x	0.10	α-cellulose			24
g-C_3N_4-Na^{6+} 3 wt% Pt	0.04	α-cellulose			25
Pt/$ZnIn_2S_4$	0.30	cellulose			26
$Ni(OH)_2$/$Cd_{0.5}Zn_{0.5}S$	1.90	waste straw			27

Catalysts	H_2 evolution rate (mmol h^{-1} g^{-1})	Substrate	Organic acid (mmol h^{-1} g^{-1})	Furfural class (mmol h^{-1} g^{-1})	Refs.
Sv-$ZnIn_2S_4$	0.52	α-cellulose			28
Pt NP-C_3N_4	1.50	α-cellulose			29
CdS-Ru	0.82	α-cellulose			30
P25-S-Ni (2)	0.82	cellulose			31
MoS_2/TiO_2	0.07	α-cellulose			16
$SrTiO_3$-Pt	0.01	corn straw pretreatment solution			32
Pt SA-CdS	0.2	α-cellulose			33
ZnS(en)/CdS	8.89	bagasse	PA1.35; GA 4.13[a]	0.70	This work

[a]Pyruvic acid (PA), glyceric acid (GA)

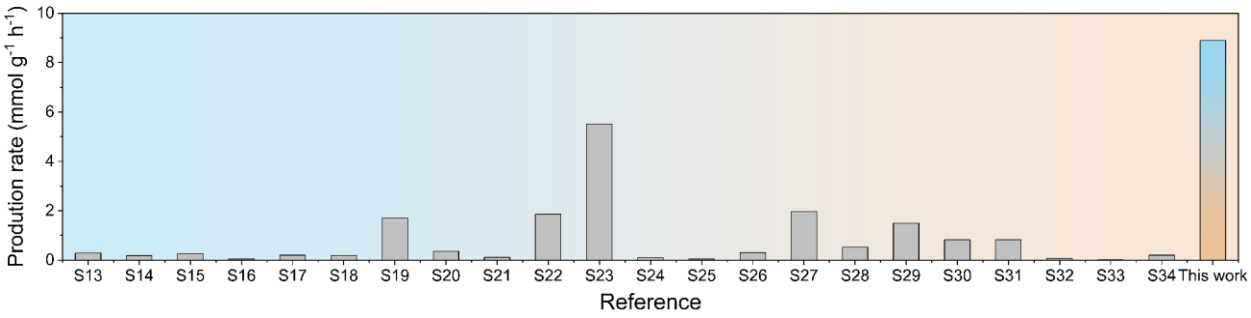

Fig. S47. Performance comparison of other polymer composite biomass materials. Comparison of hydrogen production performance from photorefining compared to other biomass sources.

Table S7 Material and life cycle inventory of pyrolysis (based on processing 1 kg of bagasse).

Unit process	Material	Value	Units
Pretreatment	Input		
	Bagasse	1	Kg
	Glycerinum	0.5003	Kg
	Water	0.4750	Kg
	Electricity	0.0100	Kwh
	Thermal energy	3.7800	MJ
	Output		
	Waste	0.2742	Kg
Pyrolysis	Input		
	Carbon dioxide	1.0600	Kg
	Biochar	0.2320	Kg
	Thermal energy	3.58	MJ
	Output		
	Biochar	0.2320	Kg
Refine	Input		
	Water	0.7950	Kg
	$Ca(OH)_2$	1.2000	Kg
	Output		
	Waste	0.6621	Kg
	$CaCO_3$	1	Kg
	Bio-oil	0.7040	Kg
	Levoglucosan	0.2134	Kg
	Steam	2.4047	Kg

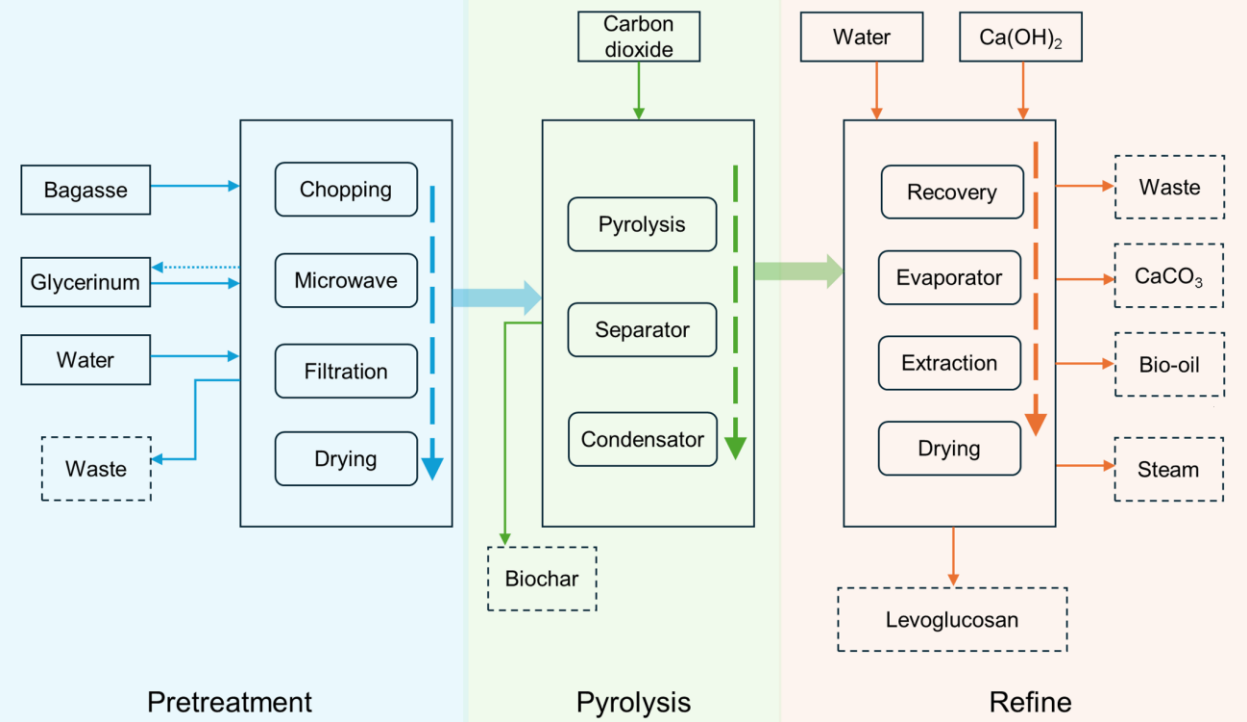

Fig. S48. System boundary diagram of the LCA process. The system boundary diagram of pyrolysis.

Table S8 Material and life cycle inventory of fermentation (based on processing 1 kg of bagasse).

Unit process	Material	Value	Units
Pretreatment		Input	
	Bagasse	1	Kg
	Sulfuric acid	0.0147	Kg
	Electricity	0.4273	Kwh
Washing		Input	
	Water	0.3397	Kg
	Electricity	2.4571	Kwh
		Output	
	Solid waste	0.7750	Kg
Fermentation		Input	
	Lime	0.0282	Kg
	Electricity	2.4571	Kg
		Output	
	Gypsum	0.0209	Kg
Refine		Input	
	Ethyl alcohol	0.3066	Kg
	Electricity	2.0897	Kwh
		Output	
	Xylitol	0.1093	Kg
	Ethanol steam	0.3066	Kg

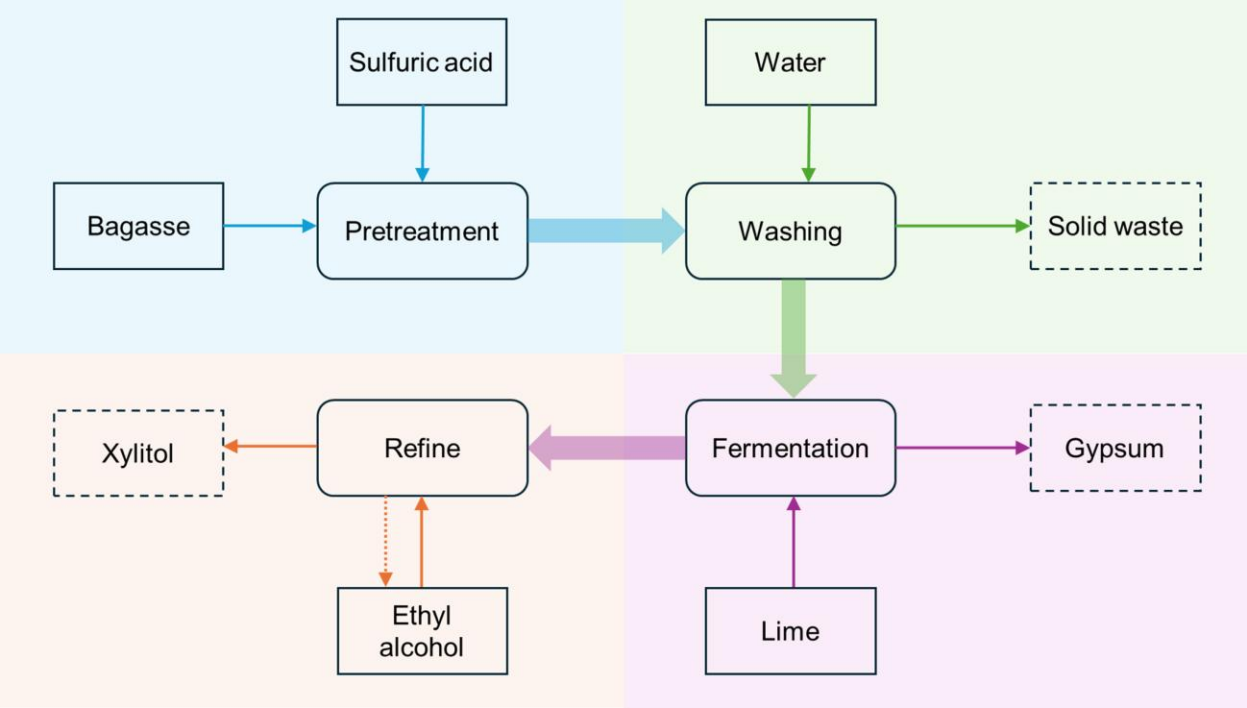

Fig. S49. System boundary diagram of the LCA process. The system boundary diagram of fermentation.

Table S9 Material and life cycle inventory data of photorefining (based on processing 1 kg of bagasse).

Unit process	Material	Value	Units
Catalysts preparation		Input	
	Cadmium acetate	0.0725	Kg
	Zinc acetate	0.1150	Kg
	Thiourea	0.1425	Kg
	Ethyl alcohol	0.1233	Kg
	Deionized water	0.1563	Kg
	Ethanediamine	0.0843	Kg
	Electricity	0.5173	Kwh
Photorefining		Input	
	Dimethyl sulfoxide	0.2750	Kg
	Bagasse	1	Kg
	Deionized water	1.25	Kg
	Sodium hydroxide	0.025	Kg
	Electricity	0.1827	Kwh
		Output	
	Hydrogen	0.0178	Kg
	Pyruvic acid	0.1189	Kg
	Glyceric acid	0.4388	Kg
	5-hydroxymethylfurfural	0.0895	Kg

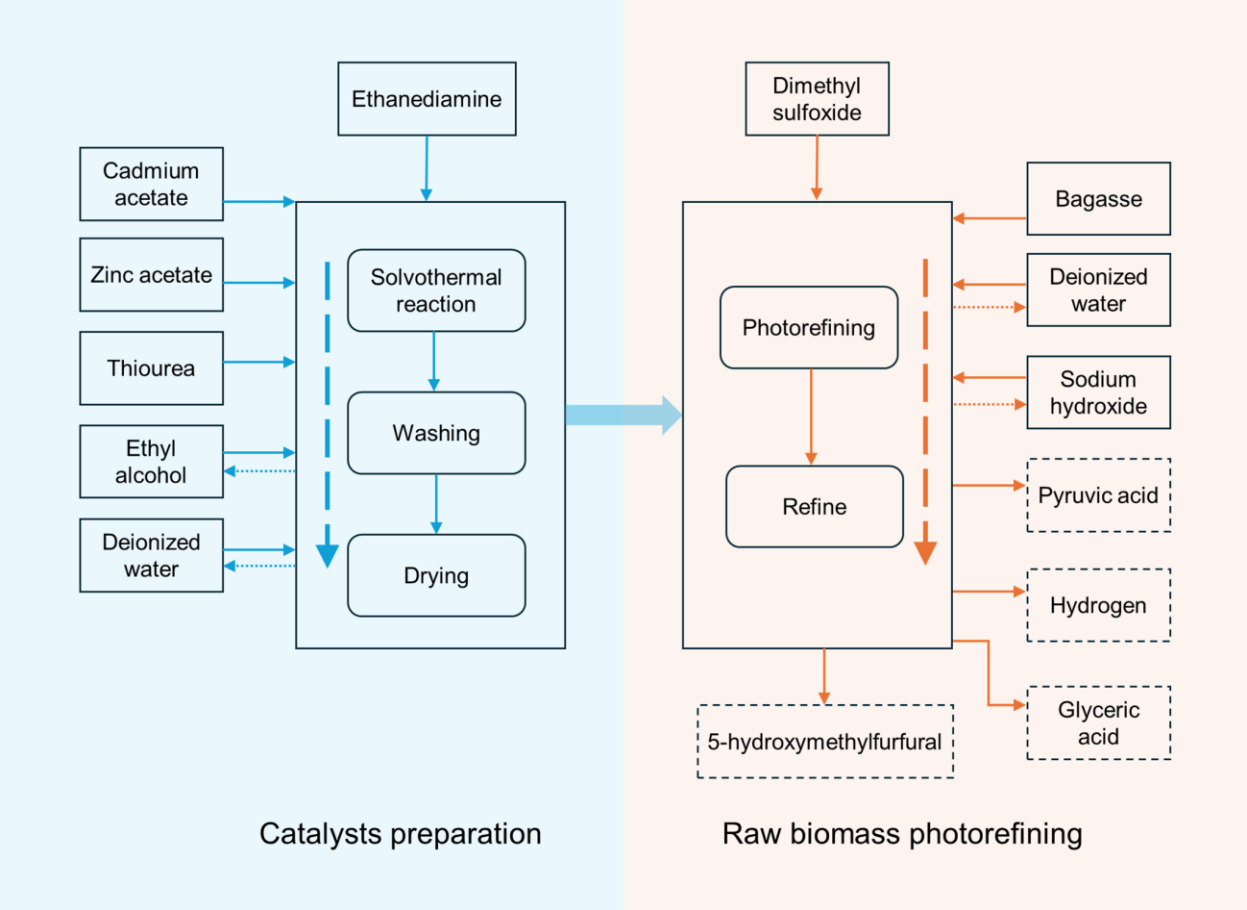

Fig. S50. System boundary diagram of the LCA process. The system boundary diagram of photorefining.

Table S10 Evaluation of the effects of pyrolysis for bagasse on the production of levoglucosan.

Impact category	Unit	Impact scores of each subprocess of conventional pyrolysis						
		Bagasse	Glycerinum	Electricity	Thermal energy	Water	$Ca(OH)_2$	Carbon dioxide
Acidification: terrestrial (AT)	kg SO_2-eq.	0.0002	0.0056	0.0001	0.0041	0.0000	0.0010	0.0021
Climate change (GWP)	kg CO_2-eq.	0.0230	1.5811	0.0329	1.7444	0.0006	1.1526	0.9993
Ecotoxicity: freshwater (EF)	kg 1,4-DCB-eq.	0.0021	0.0420	0.0018	0.0122	0	0.0023	0.0523
Ecotoxicity: marine (EM)	kg 1,4-DCB-eq.	0.0014	0.0532	0.0023	0.0194	0.0001	0.0045	0.0667
Ecotoxicity: terrestrial (ET)	kg 1,4-DCB-eq.	0.0643	3.1224	0.0399	5.7971	0.0037	2.0115	5.5594
Fossil Depletion (FDP)	kg oil-eq.	0.0026	0.2260	0.0074	0.5017	0.0002	0.1173	0.1714
Eutrophication: freshwater (EFW)	kg P-eq.	0.0000	0.0003	0.0000	0.0002	0.0000	0.0000	0.0002
Eutrophication: marine (EPM)	kg N-eq.	0.0000	0.0025	0.0000	0.0000	0.0000	0.0000	0.0000
Human toxicity: carcinogenic (HTC)	kg 1,4-DCB-eq.	0.0032	0.1418	0.0052	0.0976	0.0002	0.0205	0.1506
Human toxicity: non-carcinogenic (HNC)	kg 1,4-DCB-eq.	0.0548	1.5945	0.0423	0.5256	0.0021	0.1024	1.1553
Ionising radiation (IRD)	kbq Co-60-eq.	0.0002	0.0299	0.0015	0.0115	0.0000	0.0052	0.0354
Land use (LU)	m^2*a crop-dq.	0.0245	2.0218	0.0005	0.0072	0.0000	0.0031	0.0141
Material resources: metals/minerals (MRM)	kg Cu-dq.	0.0004	0.0323	0.0002	0.0096	0.0000	0.0156	0.0102
Ozone depletion (OD)	kg CFC-11-eq.	0.0000	0.0000	0.0000	0.0000	0.0000	0.0000	0.0000
Particulate matter formation (PMF)	kg PM2.5-eq.	0.0000	0.0020	0.0000	0.0015	0.0000	0.0004	0.0011
Photochemical oxidant formation: human health (POFH)	kg NO_x-eq.	0.0000	0.0026	0.0001	0.0024	0.0000	0.0008	0.0013
Photochemical oxidant formation: terrestrial ecosystems (POFT)	kg NO_x-eq.	0.0000	0.0028	0.0001	0.0026	0.0000	0.0008	0.0014
Water use (WU)	m^3	0.0044	0.0137	0.0001	0.0015	0.0000	0.0006	0.0047

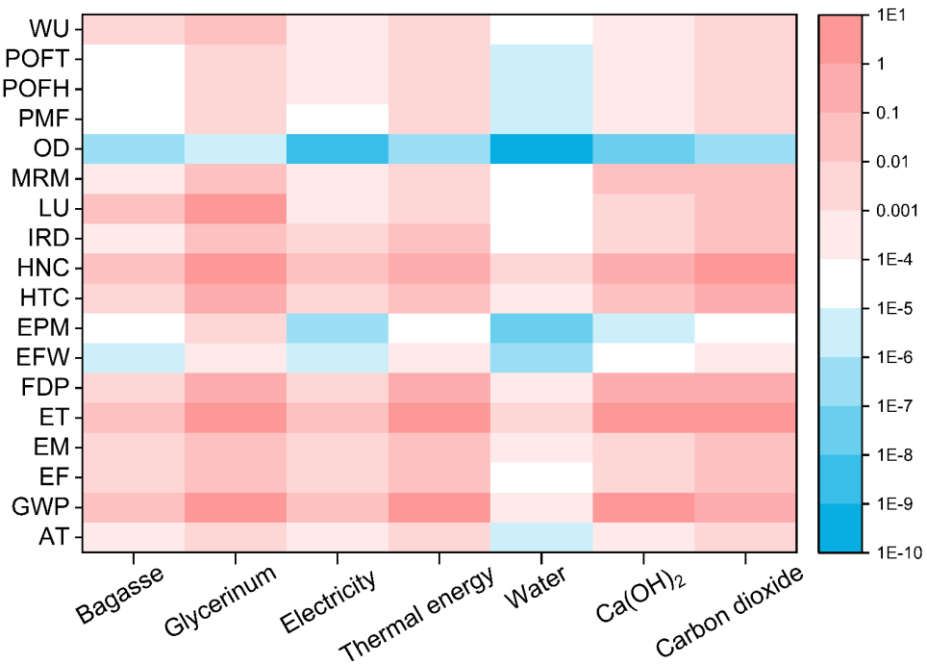

Fig. S51. Environmental scoring of process variables. Environmental scores for process variables in pyrolysis technology for bagasse.

Table S11 Evaluation of the effects of fermentation for bagasse on the production of xylito.

Impact category	Unit	Impact scores of each subprocess of conventional fermentation					
		Bagasse	Electricity	Water	Sulfuric acid	Lime	Ethyl alcohol
Acidification: terrestrial (AT)	kg SO_2-eq.	0.0002	0.0176	0.0000	0.0002	0.0000	0.0028
Climate change (GWP)	kg CO_2-eq.	0.0230	4.4679	0.0001	0.0017	0.0001	0.3413
Ecotoxicity: freshwater (EF)	kg 1,4-DCB-eq.	0.0021	0.2458	0.0000	0.0003	0.0000	0.0221
Ecotoxicity: marine (EM)	kg 1,4-DCB-eq.	0.0014	0.3142	0.0000	0.0004	0.0000	0.0197
Ecotoxicity: terrestrial (ET)	kg 1,4-DCB-eq.	0.0643	5.4143	0.0002	0.0107	0.0005	0.8440
Fossil Depletion (FDP)	kg oil-eq.	0.0026	1.0091	0.0000	0.0005	0.0000	0.0621
Eutrophication: freshwater (EFW)	kg P-eq.	0.0000	0.0009	0.0000	0.0000	0.0000	0.0000
Eutrophication: marine (EPM)	kg N-eq.	0.0000	0.0000	0.0000	0.0000	0.0000	0.0005
Human toxicity: carcinogenic (HTC)	kg 1,4-DCB-eq.	0.0032	0.7012	0.0000	0.0008	0.0000	0.0449
Human toxicity: non-carcinogenic (HNC)	kg 1,4-DCB-eq.	0.0548	5.7342	0.0002	0.0063	0.0000	0.4171
Ionising radiation (IRD)	kbq Co-60-eq.	0.0002	0.2057	0.0000	0.0001	0.0000	0.0082
Land use (LU)	m^2*a crop-dq.	0.0245	0.0649	0.0000	0.0001	0.0000	0.4807
Material resources: metals/minerals (MRM)	kg Cu-dq.	0.0004	0.0245	0.0000	0.0001	0.0002	0.0093
Ozone depletion (OD)	kg CFC-11-eq.	0.0000	0.0000	0.0000	0.0000	0.0000	0.0000
Particulate matter formation (PMF)	kg PM2.5-eq.	0.0000	0.0078	0.0000	0.0000	0.0000	0.0007
Photochemical oxidant formation: human health (POFH)	kg NO_x-eq.	0.0000	0.0137	0.0000	0.0000	0.0000	0.0010
Photochemical oxidant formation: terrestrial ecosystems (POFT)	kg NO_x-eq.	0.0000	0.0138	0.0000	0.0000	0.0000	0.0010
Water use (WU)	m^3	0.0044	0.0139	0.0000	0.0003	0.0000	0.0373

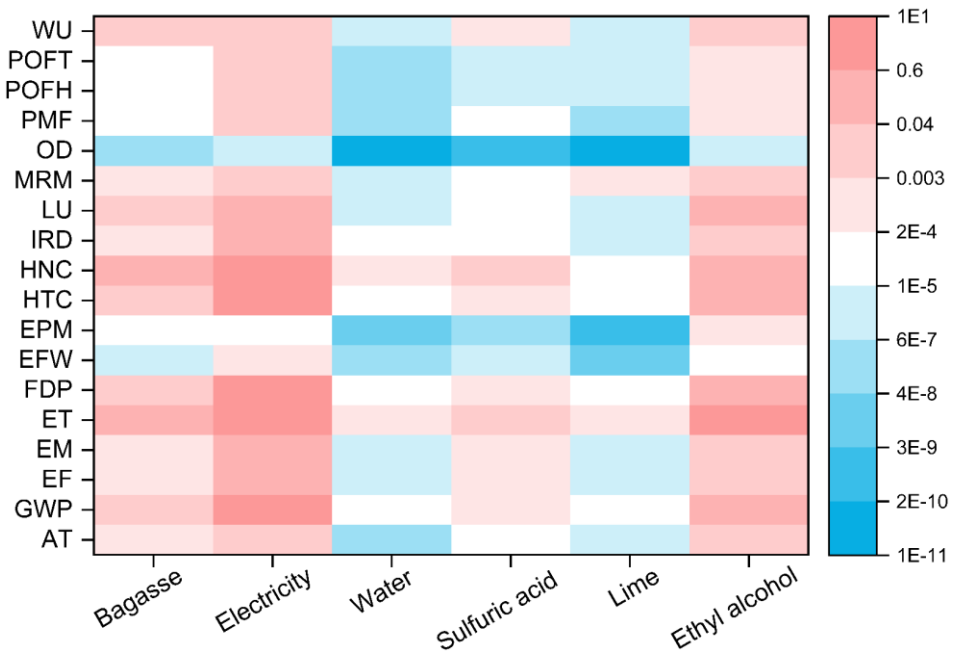

Fig. S52. Environmental scoring of process variables. Environmental scores for process variables in fermentation technology for bagasse.

Table S12 Evaluation of the effects of photorefining for bagasse on the production of platform compound.

Impact category	Unit	Impact scores of each subprocess of photorefining										
		Zinc acetate	Thiourea	Ethanediamine	Cadmium acetate	Deionized water	Ethyl alcohol	Electricity1	Bagasse	Dimethyl sulfoxide	Sodium hydroxide	Electricity2
Acidification: terrestrial (AT)	kg SO_2-eq.	0.0005	0.0028	0.0014	0.0009	0.0000	0.0011	0.0024	0.0002	0.0037	0.0001	0.0015
Climate change (GWP)	kg CO_2-eq.	0.2383	0.6175	0.5097	0.2236	0.0007	0.1373	0.6065	0.023	0.7387	0.0357	0.3882
Ecotoxicity: freshwater (EF)	kg 1,4-DCB-eq.	0.0091	0.0183	0.0202	0.1146	0.0001	0.0089	0.0334	0.0021	0.0293	0.0022	0.0214
Ecotoxicity: marine (EM)	kg 1,4-DCB-eq.	0.0144	0.0246	0.0264	0.1560	0.0001	0.0079	0.0427	0.0014	0.0385	0.0028	0.0273
Ecotoxicity: terrestrial (ET)	kg 1,4-DCB-eq.	3.4887	0.8720	0.8519	4.0398	0.0041	0.3395	0.7352	0.0643	1.0938	0.0987	0.4704
Fossil Depletion (FDP)	kg oil-eq.	0.0929	0.1719	0.1699	0.0732	0.0002	0.0250	0.1370	0.0026	0.3109	0.0092	0.0877
Eutrophication: freshwater (EFW)	kg P-eq.	0.0000	0.0002	0.0001	0.0002	0.0000	0.0000	0.0001	0.0000	0.0002	0.0000	0.0001
Eutrophication: marine (EPM)	kg N-eq.	0.0000	0.0000	0.0003	0.0000	0.0000	0.0000	0.0000	0.0000	0.0000	0.0000	0.0000
Human toxicity: carcinogenic (HTC)	kg 1,4-DCB-eq.	0.0353	0.0752	0.0779	0.0875	0.0002	0.0181	0.0952	0.0032	0.1213	0.0078	0.0609
Human toxicity: non-carcinogenic (HNC)	kg 1,4-DCB-eq.	0.4112	0.5729	0.5044	3.8792	0.0023	0.1678	0.7784	0.0548	0.7743	0.0567	0.4982
Ionising radiation (IRD)	kbq Co-60-eq.	0.0058	0.0282	0.0256	0.0225	0.0000	0.0033	0.0279	0.0002	0.0152	0.0028	0.0179
Land use (LU)	m^2*a crop-dq.	0.0029	0.0088	0.0067	0.0070	0.0000	0.1933	0.0088	0.0245	0.0099	0.0007	0.0056
Material resources: metals/minerals (MRM)	kg Cu-dq.	0.0031	0.0061	0.0141	0.0138	0.0000	0.0037	0.0033	0.0004	0.0096	0.0042	0.0021
Ozone depletion (OD)	kg CFC-11-eq.	0.0000	0.0000	0.0000	0.0000	0.0000	0.0000	0.0000	0.0000	0.0000	0.0000	0.0000
Particulate matter formation (PMF)	kg PM2.5-eq.	0.0002	0.0013	0.0006	0.0004	0.0000	0.0003	0.0011	0.0000	0.0014	0.0001	0.0007
Photochemical oxidant formation: human health (POFH)	kg NO_x-eq.	0.0004	0.0012	0.0010	0.0008	0.0000	0.0004	0.0019	0.0000	0.0012	0.0001	0.00119
Photochemical oxidant formation: terrestrial ecosystems (POFT)	kg NO_x-eq.	0.0005	0.0012	0.0011	0.0008	0.0000	0.0004	0.0019	0.0000	0.0013	0.0001	0.0012
Water use (WU)	m^3	0.0018	0.0048	0.0038	0.0039	0.0000	0.0150	0.0019	0.0044	0.0046	0.0004	0.0012

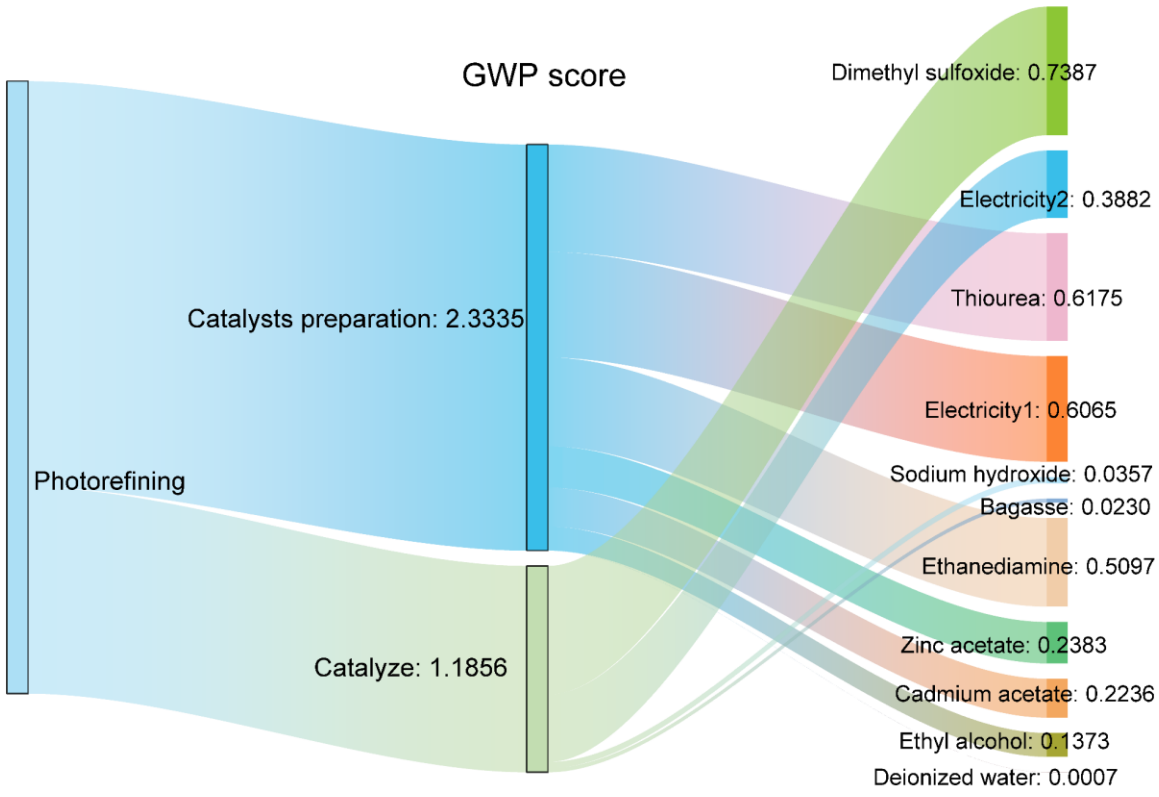

Fig. S53. GWP score of process variables. Environmental scores for process variables in photorefining technology for bagasse.

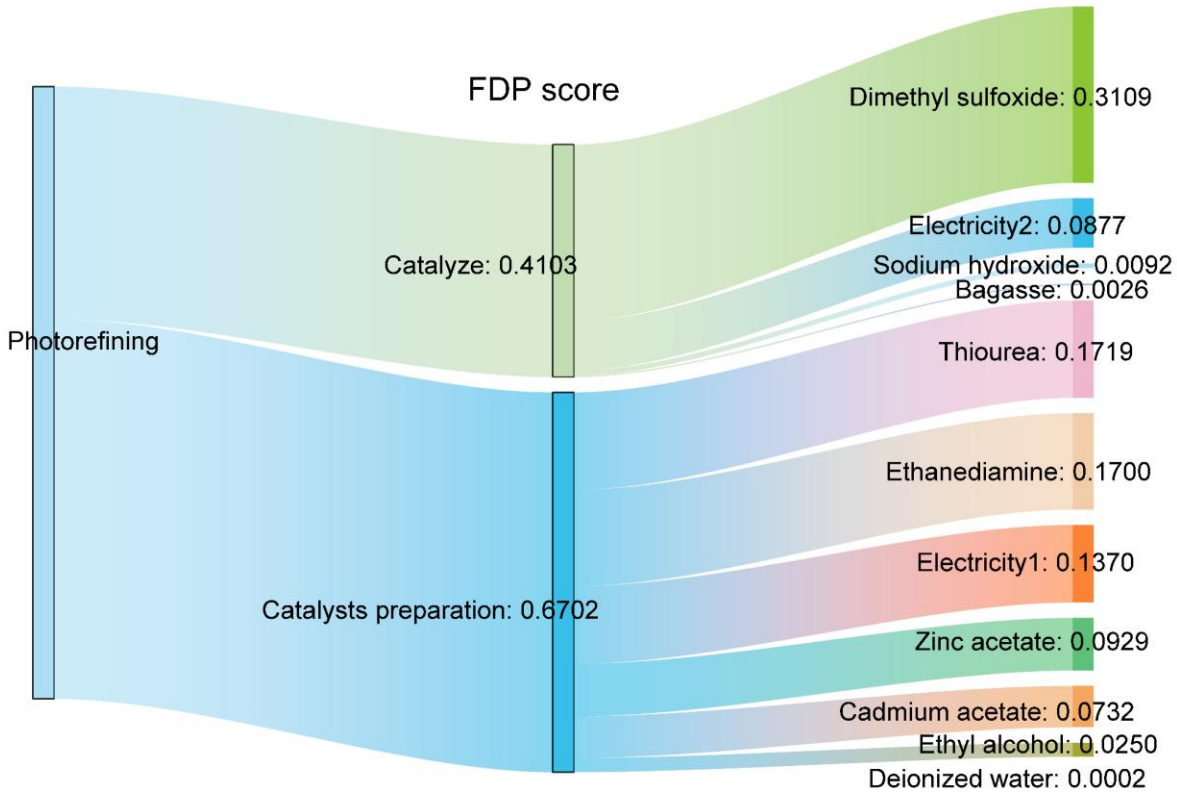

Fig. S54. FDP score of process variables. Environmental scores for process variables in photorefining technology for bagasse.

Table S13 Final environmental score for the bagasse processing technology.

Impact category	Unit	Final environmental scores for the three processes.		
		Pyrolysis	Fermentation	Photorefining
Acidification: terrestrial (AT)	kg SO_2-eq.	0.0130	0.0208	0.0132
Climate change (GWP)	kg CO_2-eq.	5.5340	4.8342	3.1309
Ecotoxicity: freshwater (EF)	kg 1,4-DCB-eq.	0.1128	0.2703	0.2381
Ecotoxicity: marine (EM)	kg 1,4-DCB-eq.	0.1476	0.3358	0.3149
Ecotoxicity: terrestrial (ET)	kg 1,4-DCB-eq.	16.5983	6.3339	11.5878
Fossil Depletion (FDP)	kg oil-eq.	1.0264	1.0743	0.9928
Eutrophication: freshwater (EFW)	kg P-eq.	0.0007	0.0010	0.0009
Eutrophication: marine (EPM)	kg N-eq.	0.0027	0.0006	0.0006
Human toxicity: carcinogenic (HTC)	kg 1,4-DCB-eq.	0.4191	0.7501	0.5217
Human toxicity: non-carcinogenic (HNC)	kg 1,4-DCB-eq.	3.4770	6.2126	7.2022
Ionising radiation (IRD)	kbq Co-60-eq.	0.0838	0.2143	0.1315
Land use (LU)	m^2*a crop-dq.	2.0711	0.5701	0.2626
Material resources: metals/minerals (MRM)	kg Cu-dq.	0.0685	0.0345	0.0585
Ozone depletion (OD)	kg CFC-11-eq.	0.0000	0.0000	0.0000
Particulate matter formation (PMF)	kg PM2.5-eq.	0.0051	0.0085	0.0054
Photochemical oxidant formation: human health (POFH)	kg NO_x-eq.	0.0074	0.0147	0.0069
Photochemical oxidant formation: terrestrial ecosystems (POFT)	kg NO_x-eq.	0.0078	0.0149	0.0073
Water use (WU)	m^3	0.0250	0.0559	0.0405

Table S14 Economic analysis of pyrolysis of bagasse.

Inventory	Value	Unit	Unit price (¥)	Total prices (¥)
Input				
Bagasse	1.0000	kg	-	-
Glycerinum	0.5003	Kg	8.6000	-4.3026
Electricity	0.0380	kWh	0.6400	-0.0241
Thermal energy	13.5300	MJ	0.0254	-0.3440
Water	1.2700	Kg	0.0052	-0.0067
$Ca(OH)_2$	1.2000	Kg	0.6030	-0.7236
Carbon dioxide	1.0600	Kg	0.2800	-0.2968
Output				
Waste	0.9363	Kg	-	-
Bio-oil	0.704	Kg	7.5	5.28
Biochar	0.232	Kg	2.67	0.61944
Levoglucosan	0.2134	Kg	35	7.469
$CaCO_3$	1	Kg	0.643	0.643
Steam	2.4047	Kg	-	-
Total revenue				8.31

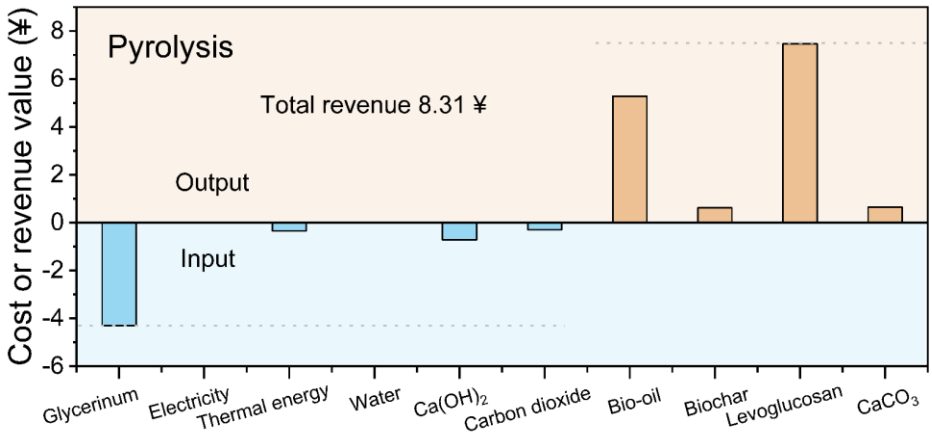

Fig. S55. Technical economic calculations for costs and benefits. Technical and economic analysis of bagasse pyrolysis technology.

Table S15 Economic analysis of fermentation of bagasse.

Inventory	Value	Unit	Unit price (¥)	Total prices (¥)
Input				
Bagasse	1	Kg	-	-
Electricity	5.1565	Kwh	0.6350	-3.2744
Water	0.3397	Kg	0.0052	-0.0018
Sulfuric acid	0.0147	Kg	0.9800	-0.0144
Lime	0.0282	Kg	0.6100	-0.0172
Ethyl alcohol	0.3066	Kg	5.8500	-1.7936
Output				
Solid waste	0.775	Kg	1.225	0.949375
Gypsum	0.0209	Kg	2.9	0.06061
Xylitol	0.1093	Kg	20	2.186
Ethanol vapor	0.3066	Kg	5.85	1.79361
Total revenue				-0.11

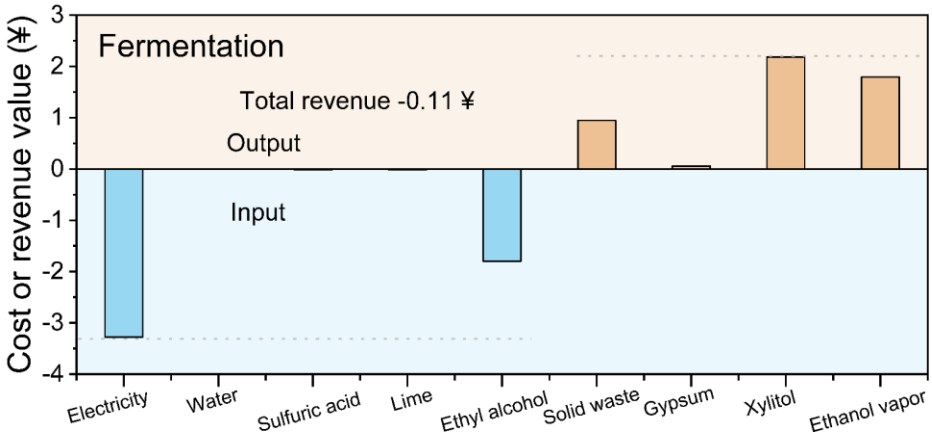

Fig. S56. Technical economic calculations for costs and benefits. Technical and economic analysis of bagasse fermentation technology.

Table S16 Economic analysis of photorefining of bagasse.

Inventory	Value	Unit	Unit price (¥)	Total prices (¥)
Input				
Zinc acetate	0.115	kg	0.75	-0.08625
Thiourea	0.1425	kg	11.56	-1.6473
Ethanediamine	0.084275	kg	10.76	-0.906799
Cadmium acetate	0.0725	kg	30	-2.175
Deionized water	0.15625	kg	0.00524	-0.00081875
Ethyl alcohol	0.123325	kg	5.85	-0.72145125
Electricity1	0.7	Kwh	0.64	-0.4445
Bagasse	1	kg		0
Deionized water	1.25	kg	0.00524	-0.00655
Dimethyl sulfoxide	0.275	kg	20.83	-5.72825
Sodium hydroxide	0.025	kg	2.7	-0.0675
Electricity2	0.448	Kwh	0.64	-0.28448
Output				
Hydrogen	0.01778	kg	29.33	0.5214874
Glyceric acid	0.43884	kg	13	5.70492
Pyruvic acid	0.11888	kg	25	2.972
5-hydroxymethylfurfura	0.08954	kg	80	7.1632
Total revenue				6.03

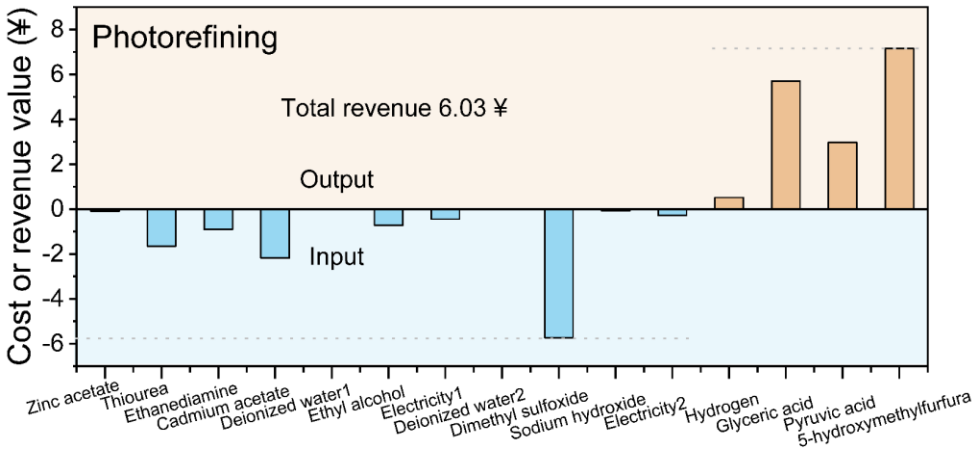

Fig. S57. Technical economic calculations for costs and benefits. Technical and economic analysis of bagasse photorefining technology.

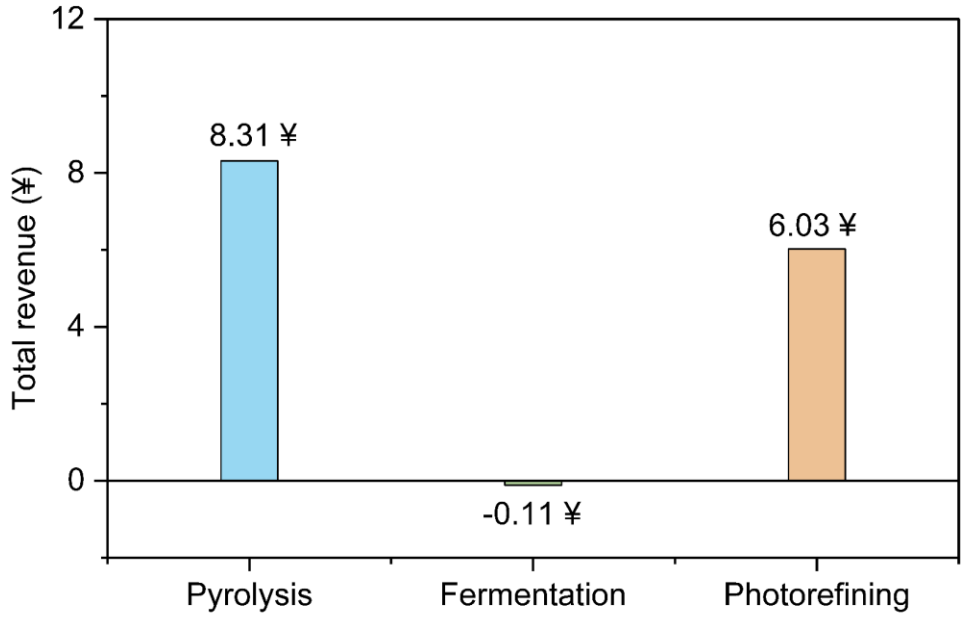

Fig. S58. Total technology revenue accounting. Comparison of the total revenue from the three technologies.

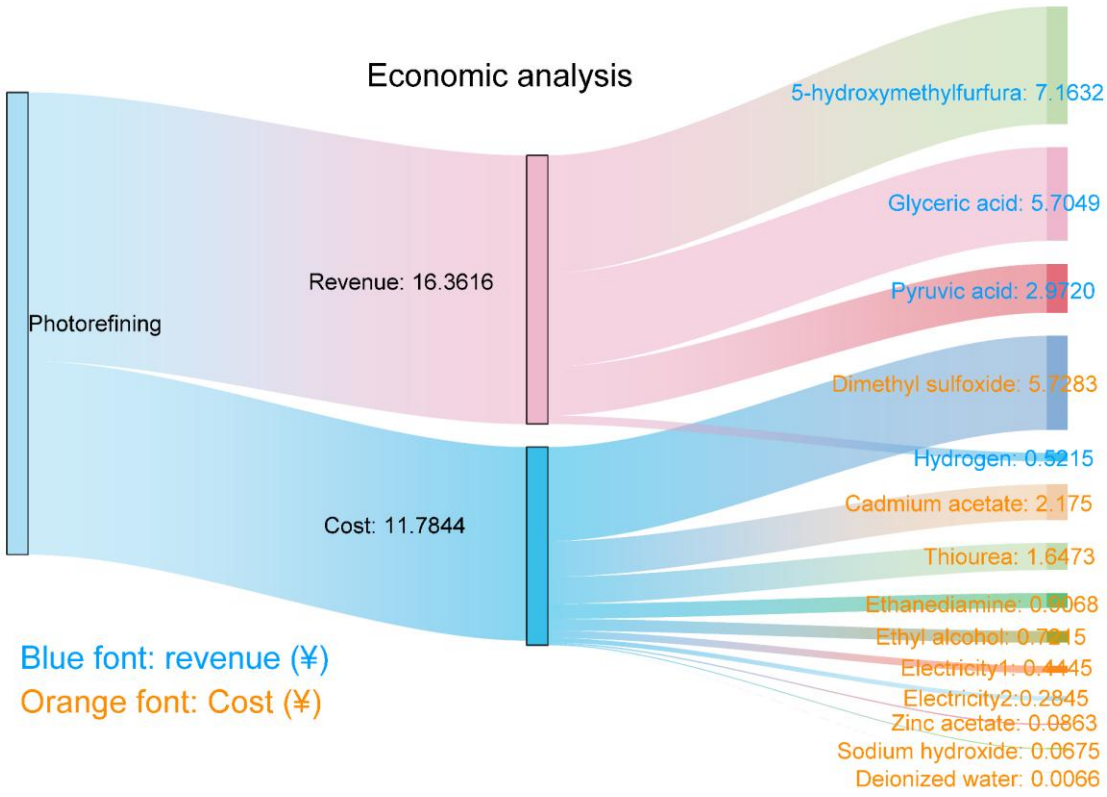

Fig. S59. Total technology revenue accounting. Cost and revenue distribution of the photorefining technology.

References

1. C. Rao, M. Xie, S. Liu, R. Chen, H. Su, L. Zhou, Y. Pang, H. Lou and X. Qiu, *ACS Appl. Mater. Interfaces*, 2021, **13**, 44243–44253.
2. A. Speltini, M. Sturini, D. Dondi, E. Annovazzi, F. Maraschi, V. Caratto, A. Profumo and A. Buttafava, *Photoch. Photobio. Sci.*, 2014, **13**, 1410–1419.
3. T. Uekert, M. A. Bajada, T. Schubert, C. M. Pichler and E. Reisner, *ChemSusChem*, 2020, **14**, 4190–4197.
4. Y. Zhou, X. Ye and D. Lin, *Int. J. Energy Res.*, 2020, **44**, 4616–4628.
5. F. Ding, H. Yu, R. Tu, S. Li, L. Chen, B. Li, J. Guo and C. Wu, *Chem. Eng. J.*, 2024, **496**, 154260.
6. H. Nagakawa and M. Nagata, *Adv. Mater. Interfaces*, 2021, **9**, 2101581.
7. J.-H. Wang, Y. Chen, J.-P. Tang, Z.-Y. Wang, Y.-H. Hu, X. Han, B.-Y. Gao, Y.-J. Yuan and Z.-T. Yu, *ACS Catal.*, 2025, **15**, 13516–13525.
8. W. Li, W. Chen, J. Guo and C. Wu, *New J. Chem.*, 2025, **49**, 2372–2381.
9. Y.-H. Hu, J.-H. Wang, Y. Chen, J.-P. Tang, Z.-Y. Wang and Y.-J. Yuan, *J. Mater. Chem. A*, 2025, **13**, 13402–13409.
10. J.-P. Tang, Y. Chen, Z.-Y. Wang, Y.-H. Hu, J.-H. Wang, L. Bao, Z.-Y. Zhao and Y.-J. Yuan, *ACS Catal.*, 2024, **15**, 265–274.
11. M. Aljohani, L. Lan, H. Daly, P. Verdía Barbará, M. Hu, S. Nisar, S. Ding, J. Hallett, N. Watkins, W. J. Macalpine, R. Rowe, A. Brandt-Talbot, G. Sanford, J. Ralph, S. D. Mansfield, C. D'Agostino, X. Fan and C. Hardacre, *J. Am. Chem. Soc.*, 2025, **147**, 29679–29686.

12. D. W. Wakerley, M. F. Kuehnel, K. L. Orchard, K. H. Ly, T. E. Rosser and E. Reisner, *Nat. Energy*, 2017, **2**, 17021.

13. Q. Cheng, Y.-J. Yuan, R. Tang, Q.-Y. Liu, L. Bao, P. Wang, J. Zhong, Z. Zhao, Z.-T. Yu and Z. Zou, *ACS Catal.*, 2022, **12**, 2118–2125.

14. X. Wu, H. Zhao, M. A. Khan, P. Maity, T. Al-Attas, S. Larter, Q. Yong, O. F. Mohammed, M. G. Kibria and J. Hu, *ACS Sustainable Chem. Eng.*, 2020, **8**, 15772–15781.

15. D. S. Achilleos, W. Yang, H. Kasap, A. Savateev, Y. Markushyna, J. R. Durrant and E. Reisner, *Angew. Chem. Int. Ed*, 2020, **59**, 18184–18188.

16. P. Wang, Y. J. Yuan, Q. Y. Liu, Q. Cheng, Z. K. Shen, Z. T. Yu and Z. Zou, *ChemSusChem*, 2021, **14**, 2860–2865.

17. L. Guan, G. Cheng, B. Tan and S. Jin, *Chem. Commun.*, 2021, **57**, 5147–5150.

18. C. M. Pichler, T. Uekert and E. Reisner, *Chem. Commun.*, 2020, **56**, 5743–5746.

19. H. Kasap, D. S. Achilleos, A. Huang and E. Reisner, *J. Am. Chem. Soc.*, 2018, **140**, 11604–11607.

20. H. Nagakawa and M. Nagata, *ACS Appl. Mater. Interfaces*, 2021, **13**, 47511–47519.

21. Q.-Y. Liu, H.-D. Wang, Y.-J. Yuan, R. Tang, L. Bao, Z. Ma, J. Zhong, Z.-T. Yu and Z. Zou, *Chem. Commun.*, 2021, **57**, 9898–9901.

22. Y. You, S. Chen, J. Zhao, J. Lin, D. Wen, P. Sha, L. Li, D. Bu and S. Huang, *Adv. Mater.*, 2023, **36**, 2307962.

23. F. Liu, Y. Fu, K. Lu, S. Wang, B. Wang, J. Huang, X. Yan, Y. Zheng, L. Guo and M. Liu, *ACS Catal.*, 2023, **13**, 15591–15602.

24. Z.-K. Xie, Y.-J. Jia, Y.-Y. Huang, D.-B. Xu, X.-J. Wu, M. Chen and W.-D. Shi, *ACS Catal.*, 2023, **13**, 13768–13776.

25. H. Luo, Y. Jia, Z. Xie and W. Shi, *Chem. Eng. Sci.*, 2024, **299**, 120409.

26. J. He, Z. Yang, Z. Wang, J. Qiu and J. Ran, *Energy Convers. Manage.*, 2024, **314**, 118634.

27. Z. Li, F. Liu, X. Yan, Y. Wang, K. Lu, J. Liu, Y. Qiao and M. Liu, *Int. J. Hydrogen Energy*, 2024, **69**, 234–241.

28. J. He, Z. Yang, Z. Wang, L. Gu, J. Qiu and J. Ran, *Chem. Eng. J.*, 2025, **503**, 158433.

29. E. Wang, Y.-C. Chu, W. Zhang, Y. Wei, C. Si, R. Palkovits, X.-P. Wu and Z. Chen, *Chinese J. Catal.*, 2025, **74**, 308–318.

30. Z. Cao, M. Tian, Q. Tang, Q. Wan, F. Ge, E. Cui, K. Song, K. Zhang, X. Wu, A. Li, W. Jiang and G. Liu, *Nano Energy*, 2025, **142**, 111180.

31. H. Hao, L. Zhang, W. Wang and S. Zeng, *ChemSusChem*, 2018, **11**, 2810–2817.

32. W. Wang, Z. Jin, B. Cheng and M. Zhao, *RSC Sustain.*, 2024, **2**, 2910–2920.

33. X. Li, Z. Su, H. Jiang, J. Liu, L. Zheng, H. Zheng, S. Wu and X. Shi, *Small*, 2024, **20**, 2400617.